Acta Cryst. (1997). B53, 203–220

A Modulation Wave Approach to the Structural Characterization of Three New Cristobalite-Related Sodium Magnesiosilicates

RAY L. WITHERS,[a]* CHARLENE LOBO,[a] JOHN G. THOMPSON,[a] SIEGBERT SCHMID[a] AND ROBERT STRANGER[b]

[a]*Research School of Chemistry, The Australian National University, Canberra ACT 0200, Australia, and* [b]*Department of Chemistry, The Faculties, Australian National University, Canberra ACT 0200, Australia. E-mail: withers@rschp1.anu.edu.au*

(Received 4 April 1996; accepted 3 October 1996)

Abstract

The crystal structures of three new cristobalite-related sodium magnesiosilicates [Na_2MgSiO_4, $M_r = 162.37$, orthorhombic, $Pna2_1$, $a = 10.835\,(5)$, $b = 5.279\,(12)$, $c = 7.067\,(8)$ Å, $D_x = 2.668$ g cm^{-3}, $Z = 4$, Cu $K\alpha$, $\lambda = 1.5418$ Å, $\mu = 75.96$ cm^{-1}, $F(000) = 319.87$; $Na_{1.74}Mg_{0.79}Al_{0.15}Si_{1.06}O_4$, $M_r = 157.02$, orthorhombic, $Pbca$, $a = 10.487\,(7)$, $b = 14.351\,(4)$, $c = 5.243\,(6)$ Å, $D_x = 2.643$ g cm^{-3}, $Z = 8$, Cu $K\alpha$, $\lambda = 1.5418$ Å, $\mu = 76.70$ cm^{-1}, $F(000) = 619.04$; $Na_{1.8}Mg_{0.9}Si_{1.1}O_4$, $M_r = 158.15$, tetragonal, $P4_12_12$, $a = 5.330\,(6)$, $c = 7.086\,(5)$ Å, $D_x = 2.609$ g cm^{-3}, $Z = 2$, Cu $K\alpha$, $\lambda = 1.5418$ Å, $\mu = 75.44$ cm^{-1}, $F(000) = 155.94$] are determined by Rietveld refinement from X-ray powder diffraction data. Plausible starting models were derived from a modulation wave approach based on the ideal C9 structure type and assuming regular SiO_4 and MgO_4 tetrahedra.

1. Introduction

The ideal $Fd3m$, SiO_2-cristobalite, or C9, structure type (Wyckoff, 1925; see Fig. 1*a*) is a high-symmetry corner-connected SiO_4 tetrahedral framework structure to which a large family of compounds, *e.g.* $A^{3+}B^{5+}O_4$-type compounds (Kosten & Arnold, 1980) are topologically closely related (O'Keeffe & Hyde, 1976, and references therein). Partial replacement of the Si^{4+} ions in the framework structure by ions of lower valence, *e.g.* Al^{3+} or Mg^{2+}, generates the so-called stuffed C9 derivative structures (Buerger, 1954) in which charge balance is maintained by alkali metals, typically Na^+ or K^+, occupying ideally 12-coordinate interstitial sites in the tetrahedral framework (see Fig. 1*b*).

Like its octahedral corner-connected counterpart perovskite (Bärnighausen, 1980), the C9 structure type represents an ideal parent structure or aristotype from which many lower-symmetry derivative structures can be obtained *via* appropriate rotation of essentially rigid framework polyhedra (tetrahedral in the case of C9-related structures and octahedral in the case of perovskite-related structures). Examples of such derivative structure types include the low cristobalite structure type (Dollase, 1965; Bertaut, Delapalme, Bassi, Durif-Varambon & Joubert, 1965), the low carnegieite, $NaAlSiO_4$, structure type (Withers & Thompson, 1993), the β-$NaFeO_2$ structure type (Bertaut & Blum, 1954),

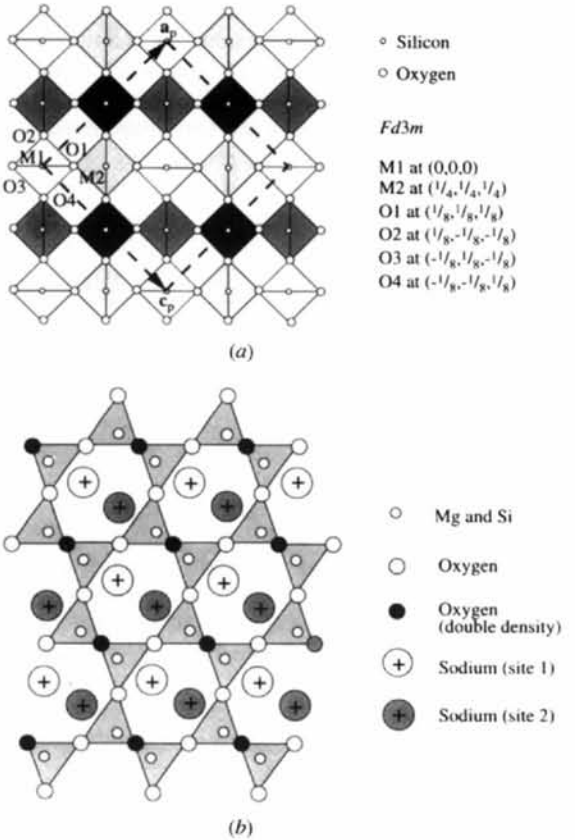

Fig. 1. An (*a*) <001> projection of the ideal $Fd3m$, SiO_2-cristobalite, or C9, structure type. Partial replacement of the Si^{4+} ions in such a framework structure by ions of lower valence such as Mg^{2+} leads to so-called 'stuffed' C9 structures in which charge balance is maintained by alkali metals such as Na^+ occupying ideally 12-coordinate interstitial sites, as shown in the <110> projection of (*b*).

© 1997 International Union of Crystallography
Printed in Great Britain – all rights reserved

the Na_2ZnSiO_4 structure type (Joubert-Bettan, Lachenal, Bertaut & Parthé, 1969) and the potassium gallate, $KGaO_2$, structure type (Vielhaber & Hoppe, 1969). All these cristobalite-related structures can be described as compositional and displacively modulated variants of the C9 structure type and can be derived therefrom *via* coupled rotations of the framework tetrahedra about two mutually orthogonal $<110>_p$ (p for parent) axes and appropriate compositional ordering. [In this paper, for consistency with our earlier paper on low carnegieite (Withers & Thompson (1993), and in order to be able to spell out the relationship between the three phases clearly, these two mutually orthogonal $<110>_p$ axes are chosen to be $[101]_p$ and $[\bar{1}01]_p$, respectively.]

Such coupled tetrahedral edge rotations invariably enlarge the original primitive parent unit cell and hence give rise to additional satellite reflections (at $\mathbf{G}_p \pm \mathbf{q}$) accompanying the strong Bragg reflections (at $\mathbf{G}_p$) characteristic of the underlying C9 parent structure. (Necessarily accompanying such compositional and displacive modulation is strain deformation.) The changes in fractional coordinates and occupancies of the resultant structure with respect to its underlying C9-type parent structure can be described in terms of compositional and displacive modulation waves associated with each of the observed independent modulation wavevectors $\mathbf{q}$ (two modulation wavevectors are here considered to be independent if they cannot be related *via* an allowed parent Bragg reflection $\mathbf{G}_p$), always remembering to allow for the possibility of a $\mathbf{q} = 0$ modulation wave.

If, as is often the case, single crystal specimens of such phases cannot be obtained, it becomes necessary to refine their structure *via* Rietveld refinement using powder data. Given that there are usually far too many parameters to be determined *via* unconstrained Rietveld refinement, it is essential to be able to derive a plausible starting model for the structures before beginning Rietveld refinement. Good starting models for the corner-connected tetrahedral framework part of such structures can be derived from the above modulation wave approach (under the crystal chemically reasonable assumption of regularly sized framework tetrahedra) provided the resultant space-group symmetry and unit-cell dimensions can be reliably determined. Such a 'modulation wave approach' to the description of cristobalite-related superstructures has, for example, recently been successfully applied to the structural parameterization and subsequent Rietveld refinement of low carnegieite (Withers & Thompson, 1993).

The same approach is utilized here in order to undertake the structure determination of three distinct cristobalite-related sodium magnesiosilicates (with compositions Na_2MgSiO_4, $Na_{1.74}Mg_{0.79}Al_{0.15}Si_{1.06}O_4$ and $Na_{1.8}Mg_{0.9}Si_{1.1}O_4$) synthesized at relatively low temperatures from reactive starting materials. Earlier work (Shannon, 1979; Shannon & Berzins, 1979) on a phase of composition Na_2MgSiO_4 reported an orthorhombic structure with space group $Pmn2_1$ and unit-cell dimensions a = 7.050 (1), b = 10.897 (1) and c = 5.290 (1) Å. Subsequently, Baur, Ohta & Shannon (1981) refined the structure of a twinned hydrothermally grown crystal of the same material in space group $P1n1$, a = 7.015 (2), b = 10.968 (2), c = 5.260 (1) Å and β = 89.97°.

In addition to this phase of composition Na_2MgSiO_4, Foris, Zumsteg & Shannon (1979) also reported the formation of an orthorhombic phase with apparent composition $Na_4Mg_2Si_3O_{10}$ ($Na_{1.6}Mg_{0.8}Si_{1.2}O_4$) and unit-cell dimensions a = 10.585 (8), b = 14.331 (8) and c = 5.233 (4) Å. They also reported samples with a slight sodium deficiency which were indexed to a tetragonal unit cell with dimensions $a = c$ = 10.489 (3) and b = 14.337 (3) Å. These phases appear to be related to the phases of composition $Na_{1.8}Mg_{0.9}Si_{1.1}O_4$ and $Na_{1.74}Mg_{0.79}Al_{0.15}Si_{1.06}O_4$ synthesized in the present work.

In this paper, electron diffraction and X-ray powder diffraction are used to determine the unit-cell dimensions and resultant space-group symmetries of these three phases. A group theoretical or modulation wave approach is then used to parameterize the structural deviation from their underlying C9 aristotypes and to derive plausible starting models for the magnesiosilicate framework, which is subsequently refined together with the interstitial sodium ions using the Rietveld method. At all stages, bond-valence sums are calculated to monitor chemical plausibility.

2. Experimental

2.1. *Synthesis*

Na_2MgSiO_4 and $Na_{1.8}Mg_{0.9}Si_{1.1}O_4$ were prepared by a sol–gel synthesis method. In each case a gel of the required stoichiometry was prepared by the addition at 313 K of concentrated solutions containing $NaNO_3$ and $MgNO_3$ (both AR grade) to a solution of colloidal silica (Ludox AM, du Pont) while stirring, resulting in the rapid formation of a gel-like precipitate. The gels were dehydrated at 403 K and the resultant white solids ground into fine powders. The powders were pressed into pellets and fired in air. Single-phase Na_2MgSiO_4 was produced by firing the pellet at 1273 K for 5 d, whereas single-phase $Na_{1.8}Mg_{0.9}Si_{1.1}O_4$ was produced by firing at 1073 K for 2 d, remixing and repelleting then firing for a further 7 d at the same temperature.

$Na_{1.74}Mg_{0.79}Al_{0.15}Si_{1.06}O_4$ was prepared by reaction of $NaNO_3$ with the magnesiosilicate mineral, talc. A naturally occurring talc of known composition was thoroughly ground with a concentrated solution of $NaNO_3$ in a mortar and pestle to form a thick slurry. Sufficient $NaNO_3$ was added to provide charge balance for Mg and Al. The slurry was dehydrated at 403 K, then ground further to produce a homogeneous fine powder. As with the sol–gel synthesis, the powder was pressed into a

pellet then fired at 1073 K for 7 d, resulting in a single-phase polycrystalline product at the stated stoichiometry.

2.2. *Characterization*

The space-group symmetries and unit-cell dimensions of the synthesized phases were determined by a combination of electron and X-ray powder diffraction. X-ray diffraction data were collected at room temperature (293 K) on a Siemens D5000 diffractometer with Cu $K\overline{\alpha}$ radiation (λ = 1.5418 Å).* Electron diffraction patterns were recorded using JEOL 100CX and Philips EM430 transmission electron microscopes. As for many such structures, beam damage in the transmission electron microscope (TEM), particularly for the $Na_{1.8}Mg_{0.9}Si_{1.1}O_4$ and $Na_{1.74}Mg_{0.79}Al_{0.15}Si_{1.06}O_4$ phases, was severe and meant that even selected-area electron diffraction patterns were very difficult to obtain.

In order to determine the compositional ordering of the framework Mg and Si atoms in the structures, solid-state ^{29}Si NMR spectroscopy was undertaken on single phase specimens. Solid-state ^{29}Si spectra were obtained using a Bruker MSL400 spectrometer operating at 79.488 MHz. Samples were spun at the magic angle at a frequency of 4.2 kHz in Bruker double air-bearing probes and the ^{29}Si spectra collected using the single pulse excitation technique with a 10 s recycle time.

2.2.1. *Electron diffraction and XRD results.* The Na_2MgSiO_4 phase was found to be orthorhombic with space-group symmetry $Pn2_1a$ (standard setting $Pna2_1$) and unit-cell dimensions a = 10.835 (5), b = 7.067 (8) and c = 5.279 (12) Å, determined *via* X-ray powder and electron diffraction (see the [100], [010] and slightly off-axis [001] zone-axis electron diffraction patterns shown in Fig. 2). In terms of the underlying C9 parent structure (see Fig. 3), $\mathbf{a} = 2\mathbf{a}' = (\mathbf{a}_p + \mathbf{c}_p)$, $\mathbf{b} = \mathbf{b}' = \mathbf{b}_p$, $\mathbf{c} = \mathbf{c}' = \frac{1}{2}(-\mathbf{a}_p + \mathbf{c}_p)$, while $\mathbf{a}^* = \frac{1}{2}\mathbf{a}'^* = \frac{1}{4}(202)^*_p$, $\mathbf{b}^* = \mathbf{b}'^* = (010)^*_p$, $\mathbf{c}^* = \mathbf{c}'^* = \frac{1}{2}(\bar{2}02)^*_p$. The additional satellite reflections which accompany the strong matrix reflections of the parent structure in the case of Na_2MgSiO_4 are therefore characterized by the independent modulation wavevectors $\mathbf{q}_1 = \frac{1}{4}(202)^*_p$, $\mathbf{q}_2 = (010)^*_p$ and $\mathbf{q}_3 = 0$. [Note that in the setting of Shannon (1979), Shannon & Berzins (1979) and Baur *et al.*

* Lists of the numbered intensity of each measured point on the profile, extended powder patterns and data for phase characterization have been deposited with the IUCr (Reference: AB0354). Copies may be obtained through The Managing Editor, International Union of Crystallography, 5 Abbey Square, Chester CH1 2HU, England.

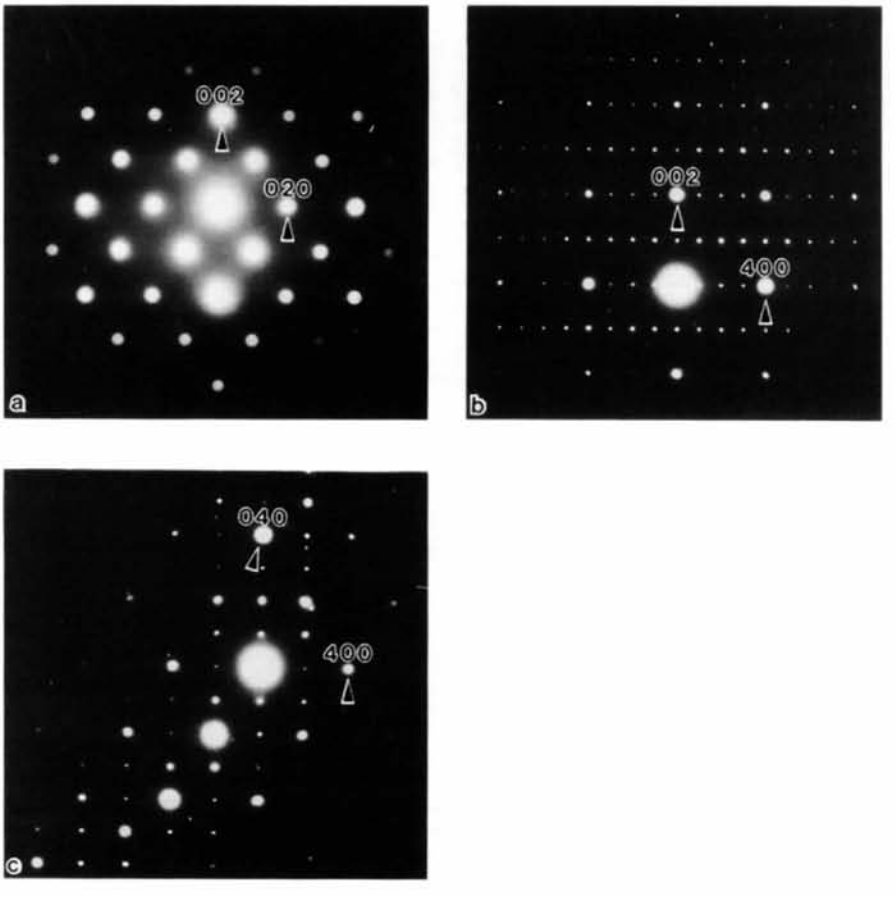

Fig. 2. (*a*) [100], (*b*) [010] and (*c*) ~ [001] electron diffraction patterns of Na_2MgSiO_4 ($Pn2_1a$ setting).

(1981), the corresponding space-group symmetry would be $P2_1nb$. Clearly the space-group symmetry required by the electron diffraction evidence is incompatible with both the $Pmn2_1$ space-group symmetry reported by Shannon (1979) and the $P1n1$ space-group symmetry reported by Baur *et al.* (1981) for Na_2MgSiO_4.]

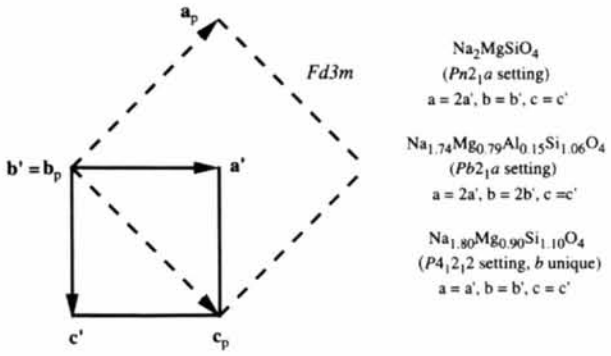

Fig. 3. The relationships between the resultant unit cells of the three newly synthesized magnesiosilicates and their underlying C9 parent structures.

The phase of composition $Na_{1.74}Mg_{0.79}Al_{0.15}Si_{1.06}O_4$ was found to be extremely sensitive to electron beam damage and it proved impossible to obtain electron diffraction patterns down all three major zone axes in order to enable an unambiguous assignment of space group. Nonetheless, from the electron diffraction patterns that were obtained, the unit-cell dimensions and Bravais lattice type could be unambiguously determined. Fig. 4, for example, shows (*a*) [010] and (*b*) <014> zone-axis electron diffraction patterns characteristic of this phase. X-ray powder diffraction suggested a tetragonal supercell with dimensions [$a = c = 10.487\,(7)$ and $b = 14.351\,(4)$ Å] very close to those previously reported by Foris *et al.* (1979). The [010] zone-axis diffraction pattern shown in Fig. 4(*a*), however, rules out tetragonal symmetry. The X-ray powder diffraction results, in conjunction with the electron diffraction results, require a primitive orthorhombic space group with unit-cell dimensions [$a = 10.487\,(7)$, $b = 14.351\,(4)$ and $c = 5.243\,(6)$ Å] reminiscent of low carnegieite (Thompson, Withers, Whittaker, Traill & Fitz Gerald, 1993).

In terms of the underlying C9 parent structure (see Fig. 3), $\mathbf{a} = 2\mathbf{a}' = (\mathbf{a}_p + \mathbf{c}_p)$, $\mathbf{b} = 2\mathbf{b}' = 2\mathbf{b}_p$, $\mathbf{c} =$

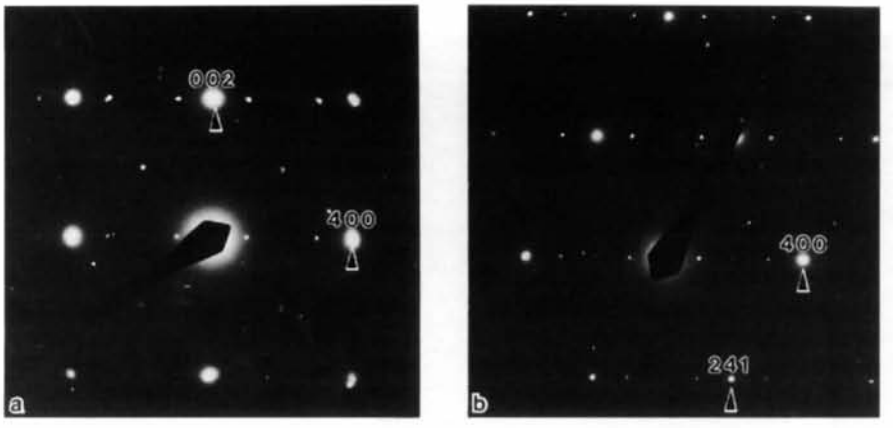

Fig. 4. (*a*) [010] and (*b*) <014> zone-axis electron diffraction patterns characteristic of $Na_{1.74}Mg_{0.79}Al_{0.15}Si_{1.06}O_4$ ($Pb2_1a$ setting).

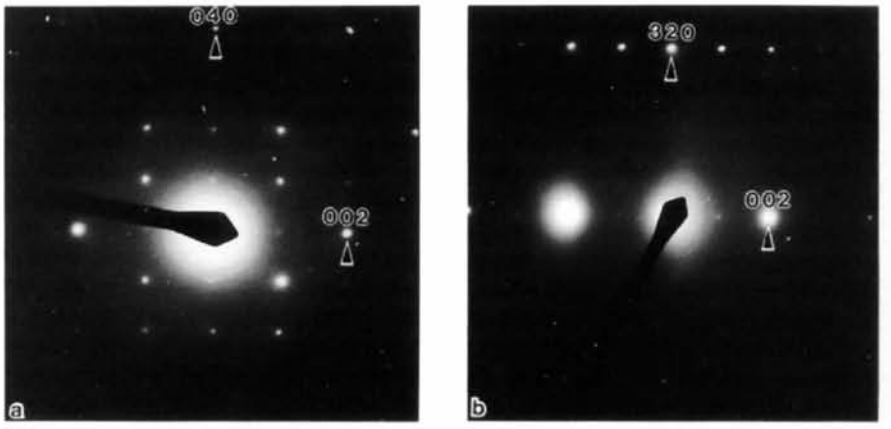

Fig. 5. (*a*) <100> and (*b*) <230> zone-axis electron diffraction patterns characteristic of $Na_{1.8}Mg_{0.9}Si_{1.1}O_4$ ($P4_12_12$, with the *b* axis corresponding to the tetragonal axis).

$\mathbf{c}' = \frac{1}{2}(-\mathbf{a}_p + \mathbf{c}_p)$, while $\mathbf{a}^* = \frac{1}{2}\mathbf{a}'^* = \frac{1}{4}(202)^*_p$, $\mathbf{b}^* = \frac{1}{2}\mathbf{b}'^* = \frac{1}{4}(020)^*_p$, $\mathbf{c}^* = \mathbf{c}'^* = \frac{1}{2}(20\bar{2})^*_p$. The additional satellite reflections which accompany the strong matrix reflections of the parent structure in the case of $Na_{1.74}Mg_{0.79}Al_{0.15}Si_{1.06}O_4$ are therefore characterized by the modulation wavevectors $\mathbf{q}_1 = \frac{1}{4}(020)^*_p$, $\mathbf{q}_2 = \frac{1}{4}(202)^*_p$, $\mathbf{q}_3 = \mathbf{q}_1 + \mathbf{q}_2 = \frac{1}{4}(222)^*_p$, $\mathbf{q}_4 = \mathbf{q}_1 - \mathbf{q}_2 = \frac{1}{4}(\bar{2}2\bar{2})^*_p$, $\mathbf{q}_5 = 2\mathbf{q}_1 = (010)^*_p$ and $\mathbf{q}_6 = 0$, as for low carnegieite (see Withers & Thompson, 1993). The relationship to low carnegieite is strengthened by the fact that the [010] zone-axis diffraction pattern shown in Fig. 4(*a*) is identical to the [010] zone-axis diffraction pattern of low carnegieite shown in Fig. 3(*c*) of Thompson *et al.* (1993). It was therefore assumed that this phase was essentially isostructural with low carnegieite, having the space group $Pb2_1a$ (standard setting $Pca2_1$) and unit-cell dimensions a = 10.487 (7), b = 14.351 (4) and c = 5.243 (6) Å.

The material of composition $Na_{1.8}Mg_{0.9}Si_{1.1}O_4$ was again found to be extremely sensitive to electron beam damage. X-ray powder diffraction suggested a tetragonal unit cell with dimensions $a = c$ = 5.330 (6) and b = 7.086 (5) Å. Electron diffraction (see, for example, the <100> and <230> zone-axis patterns shown in Fig. 5) was used to confirm the correctness of these unit-cell dimensions as well as the primitive Bravais lattice type. Taken together with the absence of extinction conditions at <100>-type zone axes (see Fig. 5*a*) and the existence of a 2_1 screw axis along **c** (as judged by the apparent absence of 00, $2l+1$, reflections in Fig. 5*b*), it would appear most likely that this phase is an analogue of low cristobalite, having space-group symmetry $P4_12_12$ and unit-cell dimensions $a = c$ = 5.330 (6) and b = 7.086 (5) Å. In terms of the underlying C9 parent structure (see Fig. 3), $\mathbf{a} = \mathbf{a}' = \frac{1}{2}(\mathbf{a}_p + \mathbf{c}_p)$, $\mathbf{b} = \mathbf{b}' = \mathbf{b}_p$, $\mathbf{c} = \mathbf{c}' = \frac{1}{2}(-\mathbf{a}_p + \mathbf{c}_p)$, while $\mathbf{a}^* = \frac{1}{2}(202)^*_p$, $\mathbf{b}^* = (010)_p{}^*$, $\mathbf{c}^* = \frac{1}{2}(\bar{2}02)^*_p$. The additional satellite reflections in the case of $Na_{1.8}Mg_{0.9}Si_{1.1}O_4$ are therefore characterized by the modulation wavevectors $\mathbf{q}_1 = (010)^*$ and $\mathbf{q}_2 = 0$.

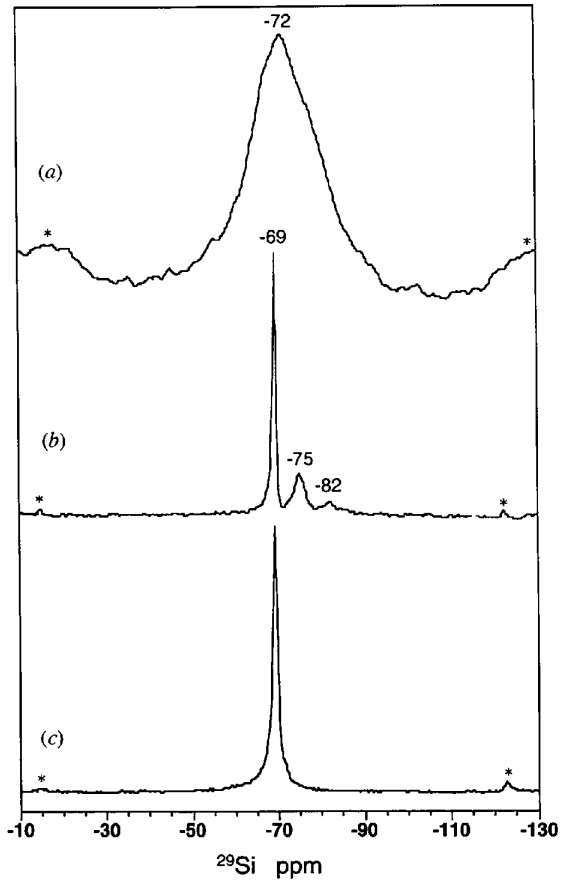

Fig. 6. ^{29}Si MAS NMR spectra of (*a*) $Na_{1.74}Mg_{0.79}Al_{0.15}Si_{1.06}O_4$, (*b*) $Na_{1.8}Mg_{0.9}Si_{1.1}O_4$ and (*c*) Na_2MgSiO_4.

2.2.2. *Solid-state ^{29}Si NMR.* The ^{29}Si NMR spectrum of Na_2MgSiO_4 (see Fig. 6*c*) contained a single sharp peak at –68.9 p.p.m. (full width at half-maximum, FWHM = 1.2 p.p.m.), consistent with exact Si/Mg ordering in the tectosilicate framework such that there exists a single Si(4Mg) environment (see Lippmaa, Mägi, Samoson, Tarmak & Engelhardt, 1981). By contrast, the broad peak at –72.0 p.p.m. (FWHM = 18.0 p.p.m.) in the ^{29}Si spectrum of $Na_{1.74}Mg_{0.79}Al_{0.15}Si_{1.06}O_4$ (Fig. 6*a*) indicates a wide range of Si environments [with a predominance of Si(3Mg) environments] consistent with significant disorder.

The ^{29}Si spectrum of $Na_{1.8}Mg_{0.9}Si_{1.1}O_4$ (see Fig. 6*b*) contains three peaks centred at –68.8 (FWHM = 0.7), –74.9 (FWHM = 3.0) and –82.1 p.p.m. (FWHM = 3.0 p.p.m.), with integrated intensities in the ratio 1:0.43:0.14. These peaks are assigned to Si(4Mg), Si(3Mg) and Si(2Mg) sites, respectively. Hence, although the sharpness of the –68.8 p.p.m. peak indicates that this phase tends towards silicon–magnesium ordering on a local scale, there is no long-range ordering of these framework metal atoms in the structure. Refinement was therefore carried out in the space group $P4_12_12$ (corresponding to a disordered structure, in which the Mg and Si atoms share the same sites) rather than the lower-symmetry space group $C222_1$, which would correspond to an ordered structure in which the magnesium and silicon sites are distinct (Kosten & Arnold, 1980).

3. A modulation wave approach

3.1. *The ideal C9 aristotypes*

The parent structure of all three of these magnesiosilicates is a stuffed C9 structure, in which some proportion of the 12-coordinate interstitial sites are filled by sodium ions in order to balance the negative charge created by partial substitution of silicon by magnesium (Fig.

1). This C9 parent structure has space-group symmetry *Fd3m* with fractional coordinates of the eight independent atoms per primitive parent unit cell given by

$M1$ in (8*a*) at (0, 0, 0)
$M2$ in (8*a*) at $(\frac{1}{4}, \frac{1}{4}, \frac{1}{4})$
Na1 in (8*b*) at $(\frac{1}{2}, \frac{1}{2}, \frac{1}{2})$
Na2 in (8*b*) at $(\frac{3}{4}, \frac{3}{4}, \frac{3}{4})$
O1 in (16*c*) at $(\frac{1}{8}, \frac{1}{8}, \frac{1}{8})$
O2 in (16*c*) at $(\frac{1}{8}, -\frac{1}{8}, -\frac{1}{8})$
O3 in (16*c*) at $(-\frac{1}{8}, \frac{1}{8}, -\frac{1}{8})$
O4 in (16*c*) at $(-\frac{1}{8}, -\frac{1}{8}, \frac{1}{8})$.

The O-atom sites are always fully occupied, whilst the average occupancies of the framework metal and sodium ion sites, given by f_{M1}^{av}, f_{M2}^{av}, f_{Na1}^{av} and f_{Na2}^{av}, in terms of the average atomic scattering factors, are dependent upon composition.

The cubic unit-cell parameter to be associated with this idealized C9 aristotype is obviously also dependent upon composition, but can be determined for any particular Mg/Si ratio *via* usage of the bond length–bond valence approach (Brown & Altermatt, 1985; Brese & O'Keeffe, 1991) in conjunction with the crystal chemically reasonable assumption that the SiO_4 and MgO_4 tetrahedra remain as regular as possible. (Note that this is undoubtedly a better assumption in the case of the SiO_4 tetrahedra than in the case of the MgO_4 tetrahedra). Ideal SiO_4, AlO_4 and MgO_4 tetrahedra have Si—O, Al—O and Mg—O tetrahedral distances given by 1.624, 1.757 and 1.949 Å, respectively [determined from the bond-valence parameters listed by Brese & O'Keeffe (1991)]. For a Mg/Si ratio of 1:1, *i.e.* for stoichiometry Na_2MgSiO_4, an ideal C9-type parent structure would then have a cubic unit-cell parameter given by $a_p = 4/3^{1/2}(1.949 + 1.624) = 8.251$ Å. The corresponding ideal cubic unit-cell parameters for $Na_{1.74}Mg_{0.79}Al_{0.15}Si_{1.06}O_4$ and $Na_{1.8}Mg_{0.9}Si_{1.1}O_4$ can likewise be determined *via* an appropriate weighting of the ideal tetrahedral *M*—O bond distances and are given by 8.140 and 8.176 Å, respectively.

3.2. *Structural deviation away from the C9 aristotypes*

Coupled rotation of the framework tetrahedra about their $<100>_{resultant} \equiv <101>_p$ tetrahedral edges (see Figs. 3 and 7) is, in a very real sense (see Withers, Thompson & Welberry, 1989), the natural 'normal mode' for such C9-related structures. Such rotation, of necessity, results in a contraction of the ideal unit-cell dimensions along the orthogonal $[010]_p$ and $<\bar{1}01>_p$ axes (see Fig. 7). The amount of contraction along these directions depends upon the magnitude of the rotation angle θ, given the reasonable assumption that the rotation angle in neighbouring <110> tetrahedral rows will have the same magnitude if not necessarily the same sign. Given a C9 parent structure, there are six possible $<101>_p$ tetrahedral edges about which such rotation might potentially take place. As mentioned in the *Introduction*, however, all the known cristobalite-related derivative structures can be derived from the C9-structure type *via* coupled rotations of the framework tetrahedra about only two (of these six possible) mutually orthogonal $<101>_p$ axes.

Strain deformation of this type, *i.e.* coupled tetrahedral edge rotation about the two mutually orthogonal $[101]_p$ and $[\bar{1}01]_p$ axes, lowers the isogonal point-group symmetry of the parent structure from cubic *m*3*m* to tetragonal 4/*mmm* or orthorhombic *mmm*, depending on the magnitudes of the rotation angles, θ_x, around $<100>_{resultant} \equiv <101>_p$ and θ_z around $<001>_{resultant} \equiv <\bar{1}01>_p$, respectively. Indeed, given the cubic aristotype unit-cell dimensions derived above, the resultant cell dimensions along **a**, **b** and **c** can be used to evaluate θ_x and θ_z [see, for example, Withers & Thompson (1993) and below]. Formally, such strain deformation is a lattice-equivalent (Bärnighausen, 1980) transformation which lowers the parent space-group symmetry (see Fig. 3) from *Fd3m* ($\mathbf{a}_p$, $\mathbf{b}_p$, $\mathbf{c}_p$) to $I4_1/amd$ [$\mathbf{a}' = \frac{1}{2}(\mathbf{a} + \mathbf{c})_p$, $\mathbf{b}' = \mathbf{b}_p$, $\mathbf{c}' = \frac{1}{2}(-\mathbf{a} + \mathbf{c})_p$] if $\theta_x = \theta_z$ or to *Imam* [$\mathbf{a}' = \frac{1}{2}(\mathbf{a} + \mathbf{c})_p$, $\mathbf{b}' = \mathbf{b}_p$, $\mathbf{c}' = \frac{1}{2}(-\mathbf{a} + \mathbf{c})_p$] if $\theta_x \neq \theta_z$.

3.3. *The modulation functions*

The structural deviation of each of the resultant structures from their underlying C9-type parent structures can be described in terms of a summation of displacive and compositional modulation waves (Pérez-Mato, Madariaga, Zúñiga & Garcia Arribas, 1987; Withers

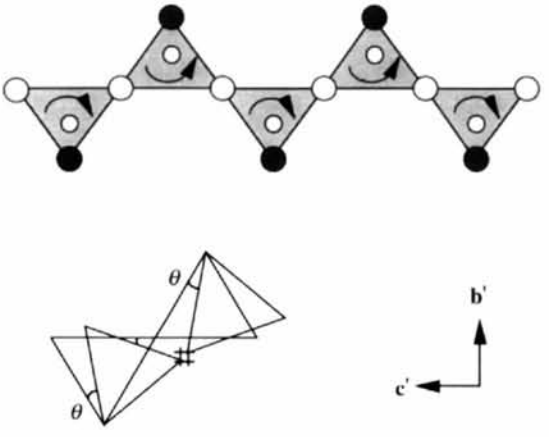

Fig. 7. Coupled rotation of the framework tetrahedra about their $<100>_{resultant} \equiv <101>_p$ tetrahedral edges is the natural 'normal mode' for C9-related structures. Such rotation results in a contraction of the ideal unit-cell dimensions along the orthogonal $[010]_p$ and $<\bar{1}01>_p$ axes. The amount of this contraction depends upon the magnitude of the rotation angle θ.

& Thompson, 1993). The displacive component of this structural deviation is given by the following expression

$$\mathbf{u}_\mu(\mathbf{T}) = \mathrm{Re}\{\Sigma_\mathbf{q}\Sigma_\alpha\alpha\varepsilon_{\mu\alpha}(\mathbf{q})\cos[2\pi\mathbf{q}.\mathbf{T} + \theta_{\mu\alpha}(\mathbf{q})]\},$$

where $\Sigma_\mathbf{q}$ represents a summation over each of the observed independent modulation wavevectors $\mathbf{q}$, $\mathbf{T}$ = a Bravais lattice translation vector of the parent C9 structure, μ = atom type, α = $\mathbf{a}_p$, $\mathbf{b}_p$ or $\mathbf{c}_p$ direction of the parent structure, and $\epsilon_{\mu\alpha}(\mathbf{q})$ and $\theta_{\mu\alpha}(\mathbf{q})$ represent the amplitude and phase of the displacive modulation wave. The position of the μth atom in the resultant structure thus being $\mathbf{r}_\mu(\mathbf{T}) = \mathbf{r}_{\mu p} + \mathbf{T} + \mu_\mu(\mathbf{T})$. Similarly, the compositional component of the structural deviation can be expressed as

$$\delta f_\mu(\mathbf{T}) = f_\mu^{\mathrm{av}}\mathrm{Re}\{\Sigma_\mathbf{q} a_\mu(\mathbf{q})\cos[2\pi\mathbf{q}.\mathbf{T} + \theta_\mu(\mathbf{q})]\},$$

where f_μ^{av} is the average atomic scattering factor of the μth site in the parent structure and $a_\mu(\mathbf{q})$ and $\theta_\mu(\mathbf{q})$ are the amplitude and phase of the compositional modulation wave.

Such modulation waves are characterized by their transformation properties under the space-group symmetry operations belonging to the little group of the corresponding modulation wavevector (Bradley & Cracknell, 1972). One or more irreducible representations compatible with the space-group symmetry of the resultant structure is associated with each observed independent modulation wavevector. Application of standard group theoretical techniques (Bradley & Cracknell, 1972) allows the irreducible representations and thus the modes of distortion compatible with the resultant space-group symmetry to be determined for each observed independent modulation wavevector. The most general possible displacement pattern $\mathbf{u}_\mu(\mathbf{T})$ for each atom in the structure can then be derived. This process is then simplified by the use of several assumptions, most notably the assumptions that the framework tetrahedra remain undistorted during the transformation and rotate through angles of the same magnitude about each rotation axis. The calculated atom shifts in the $\mathbf{a}_p$, $\mathbf{b}_p$ and $\mathbf{c}_p$ directions of the parent structure are then applied to the parent atom positions in order to generate the fractional coordinates of the atoms in the starting model for the Rietveld refinement.

4. Refinement of orthorhombic Na_2MgSiO_4

4.1. *Magnitude of the rotation about the* **a** *and* **c** *axes of the resultant structure*

Given the ideal cubic unit-cell parameter of 8.251 Å (as derived in §3.1 above), the observed cell parameters of Na_2MgSiO_4 can be used to calculate the magnitude of the rotation angles θ_z and θ_x about the **a** and **c** axes of the resultant structure (see Figs. 1*a*, 3 and 7) as follows

$$a = 2a'\cos\theta_z = 8.251(2^{1/2})\cos\theta_z$$
$$c = c'\cos\theta_x = (8.251/2^{1/2})\cos\theta_x$$
$$b = b'/(1 + \tan^2\theta_z + \tan^2\theta_x)^{1/2}$$
$$= 8.251/(1 + \tan^2\theta_z + \tan^2\theta_x)^{1/2}.$$

For rotation angles θ_x = 24.95 and θ_z = 21.50°, the predicted resultant cell parameters are 10.857, 7.045 and 5.290 Å, all within ~0.3% of their experimentally determined values. The inherent assumption that by far the major component of the structural deviation of the orthorhombic Na_2MgSiO_4 phase from its underlying C9-type parent structure is associated with tetrahedral edge rotation about the $[101]_p$ and $[\bar{1}01]_p$ axes only is thereby vindicated.

4.2. *Irreducible representations and atomic displacement patterns associated with each of the various independent modulation wavevectors*

The observed independent modulation wavevectors in the case of Na_2MgSiO_4 are $\mathbf{q}_1 = \frac{1}{4}(202)_p^*$, $\mathbf{q}_2 = (010)_p^*$ and $\mathbf{q}_3 = 0$ (the possibility of a $\mathbf{q} = 0$ modulation must always be allowed for). The determination of the structure of Na_2MgSiO_4 is equivalent to the determination of the compositional and displacement eigenvectors associated with each of these independent modulation wavevectors.

4.2.1. *The $\boldsymbol{q}_1 = \frac{1}{4}(202)_p^*$ modulation.* As a result of the *mmm* strain deformation of the C9 parent structure, the appropriate little co-group (see Ch. 3, Bradley & Cracknell, 1972) of this modulation wavevector is that sub-group of *mmm* = $\{E, C_{2c}, C_{2e}, C_{2y}, i, \sigma_{\mathrm{dc}}, \sigma_{\mathrm{de}}, \sigma_y\}$ which leaves $\mathbf{q}_1$ invariant, namely $\{E, C_{2c}, \sigma_{\mathrm{de}}, \sigma_y\}$, where the symmetry operations are defined in Fig. 1.3 of Bradley & Cracknell (1972). The irreducible representations of this little co-group are given below.

	E	C_{2c}	σ_y	σ_{de}
R_1	1	1	1	1
R_2	1	1	−1	−1
R_3	1	−1	1	−1
R_4	1	−1	−1	1

There are four one-dimensional irreducible representations labelled R_1–R_4. Only modes of R_2 and R_3 symmetry, however, are compatible with the observed resultant space-group symmetry of $Pn2_1a$.

Application of standard group theoretical techniques (see, for example, Withers & Thompson, 1993) gives the most general possible pattern of atomic displacements

associated with an R_2 irreducible representation as

$$\mathbf{u}_{M1}(\mathbf{T}) = \tfrac{1}{2}(-\mathbf{a}+\mathbf{c})_p\{\varepsilon_{Mz}(R_2;\mathbf{q}_1)\cos(2\pi\mathbf{q}_1.\mathbf{T} - 45^\circ + \varphi)\}$$
$$\mathbf{u}_{M2}(\mathbf{T}) = -\tfrac{1}{2}(-\mathbf{a}+\mathbf{c})_p\{\varepsilon_{Mz}(R_2;\mathbf{q}_1)\cos(2\pi\mathbf{q}_1.\mathbf{T} + 45^\circ + \varphi)\}$$
$$\mathbf{u}_{Na1}(\mathbf{T}) = \tfrac{1}{2}(-\mathbf{a}+\mathbf{c})_p\{\varepsilon_{Naz}(R_2;\mathbf{q}_1)\cos(2\pi\mathbf{q}_1.\mathbf{T} - 45^\circ + \varphi)\}$$
$$\mathbf{u}_{Na2}(\mathbf{T}) = -\tfrac{1}{2}(-\mathbf{a}+\mathbf{c})_p\{\varepsilon_{Naz}(R_2;\mathbf{q}_1)\cos(2\pi\mathbf{q}_1.\mathbf{T} + 45^\circ + \varphi)\}$$
$$\mathbf{u}_{O1}(\mathbf{T}) = -\tfrac{1}{2}(-\mathbf{a}+\mathbf{c})_p\{\varepsilon_{O1,3z}(R_2;\mathbf{q}_1)\cos(2\pi\mathbf{q}_1.\mathbf{T} + 90^\circ + \varphi)\}$$
$$\mathbf{u}_{O3}(\mathbf{T}) = \tfrac{1}{2}(-\mathbf{a}+\mathbf{c})_p\{\varepsilon_{O1,3z}(R_2;\mathbf{q}_1)\cos(2\pi\mathbf{q}_1.\mathbf{T} + \varphi)\}$$
$$\mathbf{u}_{O2}(\mathbf{T}) = \tfrac{1}{2}(\mathbf{a}+\mathbf{c})_p\{\varepsilon_{O2,4x}(R_2;\mathbf{q}_1)\cos(2\pi\mathbf{q}_1.\mathbf{T} - 45^\circ + \varphi)\}$$
$$\mathbf{u}_{O4}(\mathbf{T}) = -\tfrac{1}{2}(\mathbf{a}+\mathbf{c})_p\{\varepsilon_{O2,4x}(R_2;\mathbf{q}_1)\cos(2\pi\mathbf{q}_1.\mathbf{T} - 45^\circ + \varphi)\},$$

while the most general possible pattern of atomic displacements associated with the R_3 irreducible representation is given by

$$\mathbf{u}_{M1}(\mathbf{T}) = \tfrac{1}{2}(-\mathbf{a}+\mathbf{c})_p\{\varepsilon_{Mz}(R_3;\mathbf{q}_1)\cos(2\pi\mathbf{q}_1.\mathbf{T} - 45^\circ + \varphi)\}$$
$$\mathbf{u}_{M2}(\mathbf{T}) = \tfrac{1}{2}(-\mathbf{a}+\mathbf{c})_p\{\varepsilon_{Mz}(R_3;\mathbf{q}_1)\cos(2\pi\mathbf{q}_1.\mathbf{T} + 45^\circ + \varphi)\}$$
$$\mathbf{u}_{Na1}(\mathbf{T}) = \tfrac{1}{2}(-\mathbf{a}+\mathbf{c})_p\{\varepsilon_{Naz}(R_3;\mathbf{q}_1)\cos(2\pi\mathbf{q}_1.\mathbf{T} - 45^\circ + \varphi)\}$$
$$\mathbf{u}_{Na2}(\mathbf{T}) = \tfrac{1}{2}(-\mathbf{a}+\mathbf{c})_p\{\varepsilon_{Naz}(R_3;\mathbf{q}_1)\cos(2\pi\mathbf{q}_1.\mathbf{T} + 45^\circ + \varphi)\}$$
$$\mathbf{u}_{O1}(\mathbf{T}) = \tfrac{1}{2}(-\mathbf{a}+\mathbf{c})_p\{\varepsilon_{O1,3z}(R_3;\mathbf{q}_1)\cos(2\pi\mathbf{q}_1.\mathbf{T} + 180^\circ + \varphi)\}$$
$$\mathbf{u}_{O3}(\mathbf{T}) = \tfrac{1}{2}(-\mathbf{a}+\mathbf{c})_p\{\varepsilon_{O1,3z}(R_3;\mathbf{q}_1)\cos(2\pi\mathbf{q}_1.\mathbf{T} + 90^\circ + \varphi)\}$$
$$\mathbf{u}_{O2}(\mathbf{T}) = -\mathbf{b}_p\{\varepsilon_{O2,4y}(R_3;\mathbf{q}_1)\cos(2\pi\mathbf{q}_1.\mathbf{T} - 45^\circ + \varphi)\} + \tfrac{1}{2}(-\mathbf{a}+\mathbf{c})_p\{\varepsilon_{O2,4z}(R_3;\mathbf{q}_1)\cos(2\pi\mathbf{q}_1.\mathbf{T} - 45^\circ + \varphi)\}$$
$$\mathbf{u}_{O4}(\mathbf{T}) = \mathbf{b}_p\{\varepsilon_{O2,4y}(R_3;\mathbf{q}_1)\cos(2\pi\mathbf{q}_1.\mathbf{T} - 45^\circ + \varphi)\} + \tfrac{1}{2}(-\mathbf{a}+\mathbf{c})_p\{\varepsilon_{O2,4z}(R_3;\mathbf{q}_1)\cos(2\pi\mathbf{q}_1.\mathbf{T} - 45^\circ + \varphi)\}.$$

Note that condensed modes of R_2 and R_3 symmetry on their own would only guarantee a resultant space-group symmetry of $P11a$. In order to be compatible with the resultant space-group symmetry of $Pn2_1a$, the phase angle φ in the above equations must be put at zero. (It is interesting to note here that the resultant unit cell and space-group symmetry of low carnegieite and $Na_{1.74}Mg_{0.79}Al_{0.15}Si_{1.06}O_4$ also imply that modes of R_2 and R_3 symmetry alone can be associated with the modulation wavevector $\frac{1}{4}(202)^*_p$. The resultant $Pb2_1a$ space-group symmetry in these cases, however, requires that the phase angle φ in the above equations must equal 135°.

Thus, formally there are nine symmetry-allowed, independent, displacive degrees of freedom (the nine independent amplitudes ε in the above equations) associated with just this $\mathbf{q}_1$ modulation wavevector alone, seven of which are associated with the framework tetrahedra. The R_2 and R_3 modes correspond to different types of distortion of the C9 aristotype. Only the latter, R_3, mode is compatible with tetrahedral edge rotation [about the $\mathbf{a}'$ or $(\mathbf{a}+\mathbf{c})_p$ axis]; the former involves tetrahedral distortion rather than tetrahedral edge rotation and therefore the three associated parameters $\varepsilon_{Mz}(R_2;\mathbf{q}_1)$, $\varepsilon_{O1,3z}(R_2;\mathbf{q}_1)$ and $\varepsilon_{O2,4x}(R_2;\mathbf{q}_1)$ can all be assumed to be zero for the purpose of deriving a starting model for refinement. Neither mode is compatible with compositional modulation of the framework metal atoms.

The phase angles for the R_3 mode are fixed by the resultant space-group symmetry and, as expected, ensure that each tetrahedron rotates through an angle of the same magnitude in order to preserve the connectivity of the structure. The assumption that the R_3 mode is associated purely with tetrahedral edge rotation around the $\mathbf{a}'$ or $(\mathbf{a}+\mathbf{c})_p$ axes (see Figs. 1*a* and 7) requires that $\varepsilon_{O1,3z}(R_3;\mathbf{q}_1) = 0$. This leaves three displacive degrees of freedom associated with tetrahedral edge rotation about the $\mathbf{a}'$ axis, the magnitudes of which can be estimated to be $\varepsilon_{O2,4z}(R_3;\mathbf{q}_1) = 2\varepsilon_{Mz}(R_3;\mathbf{q}_1) \simeq 0.233$ and $\varepsilon_{O2,4y}(R_3;\mathbf{q}_1) = 0.123$ given a rotation angle of 24.95° about this axis. Thus, the initial seven degrees of freedom associated with the framework structure can be reduced to just 1, namely the direction in which the tetrahedron at the origin rotates. No attempt has been made to estimate the shifts associated with the sodium ions. This is because the sodium ions are not considered to be part of the tetrahedral framework in this approach and, hence, there is no simple way of tying their displacements to those of the other atoms.

4.2.2. *The $\boldsymbol{q}_2$ ($\equiv 2\boldsymbol{q}_1$) = $\boldsymbol{b}^*$ modulation.* The little co-group (see Bradley & Cracknell, 1972) of this modulation wavevector is *mmm* itself. The corresponding irreducible representations are listed in Table 1. There are eight one-dimensional irreducible representations labelled R_1 to R_8. Only modes of R_2 and R_8 symmetry, however, are compatible with the observed resultant space-group symmetry of $Pn2_1a$. Again neither mode is compatible with the compositional modulation of the framework metal atoms.

Table 1. *Irreducible matrix representations associated with* $\mathbf{q}_2 = \mathbf{b}_p^*$ *and* $\mathbf{q}_3 = \mathbf{0}$

	$\{E\|\mathbf{0}\}$	$\{C_{2y}\|\mathbf{0}\}$	$\{C_{2c}\|\frac{1}{4}(-\mathbf{a}+\mathbf{b}-\mathbf{c})_p\}$	$\{\bar{C}_{2c}\|\frac{1}{4}(\mathbf{a}+\mathbf{b}-\mathbf{c})_p\}$	$\{i\|\frac{1}{4}(-\mathbf{a}+\mathbf{b}-\mathbf{c})_p\}$	$\{\sigma_y\|\frac{1}{4}(\mathbf{a}+\mathbf{b}+\mathbf{c})_p\}$	$\{\sigma_{de}\|\mathbf{0}\}$	$\{\sigma_{dc}\|\mathbf{0}\}$
R_1	1	1	1	1	1	1	1	1
R_2	1	−1	1	−1	1	−1	1	−1
R_3	1	1	−1	−1	1	1	−1	−1
R_4	1	−1	−1	1	1	−1	−1	1
R_5	1	1	1	1	−1	−1	−1	−1
R_6	1	−1	1	−1	−1	1	−1	1
R_7	1	1	−1	−1	−1	−1	1	1
R_8	1	−1	−1	1	−1	1	1	−1

The most general patterns of atomic displacement associated with the R_2 irreducible representation is given by

$$\mathbf{u}_{M1}(\mathbf{T}) = \tfrac{1}{2}(\mathbf{a}+\mathbf{c})_p\{\varepsilon_{Mx}(R_2;\mathbf{q}_2)\cos(2\pi\mathbf{q}_2.\mathbf{T})\}$$
$$\mathbf{u}_{M2}(\mathbf{T}) = -\tfrac{1}{2}(\mathbf{a}+\mathbf{c})_p\{\varepsilon_{Mx}(R_2;\mathbf{q}_2)\cos(2\pi\mathbf{q}_2.\mathbf{T})\}$$
$$\mathbf{u}_{Na1}(\mathbf{T}) = \tfrac{1}{2}(\mathbf{a}+\mathbf{c})_p\{\varepsilon_{Nax}(R_2;\mathbf{q}_2)\cos(2\pi\mathbf{q}_2.\mathbf{T})\}$$
$$\mathbf{u}_{Na2}(\mathbf{T}) = -\tfrac{1}{2}(\mathbf{a}+\mathbf{c})_p\{\varepsilon_{Nax}(R_2;\mathbf{q}_2)\cos(2\pi\mathbf{q}_2.\mathbf{T})\}$$
$$\mathbf{u}_{O1}(\mathbf{T}) = \mathbf{u}_{O3}(\mathbf{T}) = 0$$
$$\mathbf{u}_{O2}(\mathbf{T}) = \mathbf{u}_{O4}(\mathbf{T}) = \tfrac{1}{2}(\mathbf{a}+\mathbf{c})_p\{\varepsilon_{Ox}(R_2;\mathbf{q}_2)\cos(2\pi\mathbf{q}_2.\mathbf{T})\},$$

while that associated with the R_8 irreducible representation is given by

$$\mathbf{u}_{M1}(\mathbf{T}) = \mathbf{u}_{M2}(\mathbf{T}) = \tfrac{1}{2}(\mathbf{a}+\mathbf{c})_p\{\varepsilon_{Mx}(R_8;\mathbf{q}_2)\cos(2\pi\mathbf{q}_2.\mathbf{T})\}$$
$$\mathbf{u}_{Na1}(\mathbf{T}) = \mathbf{u}_{Na2}(\mathbf{T}) = \tfrac{1}{2}(\mathbf{a}+\mathbf{c})_p\{\varepsilon_{Nax}(R_8;\mathbf{q}_2)\cos(2\pi\mathbf{q}_2.\mathbf{T})\}$$
$$\mathbf{u}_{O1}(\mathbf{T}) = \tfrac{1}{2}(\mathbf{a}+\mathbf{c})_p\{\varepsilon_{Ox}(R_8;\mathbf{q}_2)\cos(2\pi\mathbf{q}_2.\mathbf{T})\} - \mathbf{b}_p\{\varepsilon_{Oy}(R_8;\mathbf{q}_2)\cos(2\pi\mathbf{q}_2.\mathbf{T})\}$$
$$\mathbf{u}_{O3}(\mathbf{T}) = \tfrac{1}{2}(\mathbf{a}+\mathbf{c})_p\{\varepsilon_{Ox}(R_8;\mathbf{q}_2)\cos(2\pi\mathbf{q}_2.\mathbf{T})\} + \mathbf{b}_p\{\varepsilon_{Oy}(R_8;\mathbf{q}_2)\cos(2\pi\mathbf{q}_2.\mathbf{T})\}$$
$$\mathbf{u}_{O2}(\mathbf{T}) = \mathbf{u}_{O4}(\mathbf{T}) = 0.$$

The R_2 mode is incompatible with tetrahedral edge rotation and hence the amplitudes $\varepsilon_{Mx}(R_2;\mathbf{q}_2)$ and $\varepsilon_{Ox}(R_2;\mathbf{q}_2)$ can be set to zero. The R_8 mode entails displacements along both the $\mathbf{a}' = \frac{1}{2}(\mathbf{a}+\mathbf{c})_p$ and $\mathbf{b}' = \mathbf{b}_p$ directions and is therefore compatible with tetrahedral edge rotation about the $\mathbf{c}'$ axis. Given a rotation angle of 21.5° about this axis, the three displacive degrees of freedom associated with tetrahedral edge rotation about this $\mathbf{c}' = \frac{1}{2}(-\mathbf{a}+\mathbf{c})_p$ axis can be estimated to be $\varepsilon_{Ox}(R_8;\mathbf{q}_2) = 2\varepsilon_{Mx}(R_8;\mathbf{q}_2) \simeq 0.139$ and $\varepsilon_{Oy}(R_8;\mathbf{q}_2) \simeq 0.076$.

4.2.3. *The* $\mathbf{q}_3 = 0$ *modulation.* The possibility of a $\mathbf{q}_3 = 0$ modulation wave must always be allowed for. Such a modulation wave allows the average structure (*i.e.* the structure corresponding to the sub-set of strong Bragg reflections alone) to differ from the strain-deformed underlying C9 parent structure (Pérez-Mato *et al.*, 1987). The little co-group of this modulation wavevector is again *mmm*, the irreducible representations of which are also as listed in Table 1. For a $\mathbf{q} = \mathbf{0}$ modulation wavevector, only modes of R_1 and R_7 symmetry are compatible with the observed resultant space-group symmetry of $Pn2_1a$.

The R_7 mode allows both compositional and displacive modulation. The most general possible compositional ordering pattern is given by

$$f_{M1}(\mathbf{T}) = \tfrac{1}{2}(f_{Mg}+f_{Si})[1 + a_M(R_7;\mathbf{q}_3)]$$
$$f_{M2}(\mathbf{T}) = \tfrac{1}{2}(f_{Mg}+f_{Si})[1 - a_M(R_7;\mathbf{q}_3)].$$

The solid-state ^{29}Si NMR spectrum indicates that all Si atoms in the structure are surrounded by four Mg atoms and *vice versa*, *i.e.*

$$\tfrac{1}{2}(f_{Mg}+f_{Si})a_M(R_7;\mathbf{q}_3) = \tfrac{1}{2}(-f_{Mg}+f_{Si}).$$

This choice of sign for $a_M(R_7;\mathbf{q}_3)$ implies that Si is at the origin of the unit cell since $f_{M1}(\mathbf{T}) = f_{Si}$ and $f_{M2}(\mathbf{T}) = f_{Mg}$. The alternative choice of origin can be made by reversing the signs of $a_M(R_7;\mathbf{q}_3)$ in the above equations. The associated displacive modulation associated with this R_7 mode is given by

$$\mathbf{u}_{M1}(\mathbf{T}) = \mathbf{u}_{M2}(\mathbf{T}) = \mathbf{b}_p\varepsilon_{My}(R_7;\mathbf{q}_3)$$
$$\mathbf{u}_{Na1}(\mathbf{T}) = \mathbf{u}_{Na2}(\mathbf{T}) = \mathbf{b}_p\varepsilon_{Nay}(R_7;\mathbf{q}_3)$$
$$\mathbf{u}_{O1}(\mathbf{T}) = -\tfrac{1}{2}(\mathbf{a}+\mathbf{c})_p\varepsilon_{O1,3x}(R_7;\mathbf{q}_3) - \mathbf{b}_p\varepsilon_{O1,3y}(R_7;\mathbf{q}_3)$$
$$\mathbf{u}_{O3}(\mathbf{T}) = \tfrac{1}{2}(\mathbf{a}+\mathbf{c})_p\varepsilon_{O1,3x}(R_7;\mathbf{q}_3) - \mathbf{b}_p\varepsilon_{O1,3y}(R_7;\mathbf{q}_3)$$
$$\mathbf{u}_{O2}(\mathbf{T}) = \mathbf{b}_p\varepsilon_{O2,4y}(R_7;\mathbf{q}_3) + \tfrac{1}{2}(-\mathbf{a}+\mathbf{c})_p\varepsilon_{O2,4z}(R_7;\mathbf{q}_3)$$
$$\mathbf{u}_{O4}(\mathbf{T}) = \mathbf{b}_p\varepsilon_{O2,4y}(R_7;\mathbf{q}_3) - \tfrac{1}{2}(-\mathbf{a}+\mathbf{c})_p\varepsilon_{O2,4z}(R_7;\mathbf{q}_3).$$

This pattern of atomic displacements is incompatible with tetrahedral edge rotation about either the $\mathbf{a}' = \frac{1}{2}(\mathbf{a}+\mathbf{c})_p$ or $\mathbf{c}' = \frac{1}{2}(-\mathbf{a}+\mathbf{c})_p$ axes and hence $\varepsilon_{My}(R_7;\mathbf{q}_3)$ can be set at zero. The compositional ordering of the framework metal atoms, however, requires that the associated shifts of the O atoms be non-zero, in order to describe the alternate expansion and contraction of the MgO_4 and SiO_4 tetrahedra relative to the average tetrahedral size (the ideal Mg—O and Si—O bond distances are

Table 2. *Group theoretically derived fractional coordinates for orthorhombic phase ($Pn2_1a$)*

Atom type	x	y	z
$M1(\mathbf{T}=0)$	$0+\frac{1}{2}\varepsilon_{Mx}(R_8;\mathbf{q}_2)$	0	$0+1/[2^{1/2}\varepsilon_{Mz}(R_3;\mathbf{q}_1)]$
$M2(\mathbf{T}=0)$	$\frac{1}{4}+\frac{1}{2}\varepsilon_{Mx}(R_8;\mathbf{q}_2)$	$\frac{1}{4}$	$0+1/[2^{1/2}\varepsilon_{Mz}(R_3;\mathbf{q}_1)]$
$Na1(\mathbf{T}=0)$	0	$\frac{1}{2}$	0
$Na2(\mathbf{T}=0)$	$\frac{1}{4}$	$-\frac{1}{4}$	0
$O1(\mathbf{T}=0)$	$\frac{1}{8}+\frac{1}{2}\varepsilon_{Ox}(R_8;\mathbf{q}_2)-\frac{1}{2}\varepsilon_{O1,3x}(R_7;\mathbf{q}_3)$	$\frac{1}{8}-\varepsilon_{Oy}(R_8;\mathbf{q}_2)-\varepsilon_{O1,3y}(R_7;\mathbf{q}_3)$	0
$O2(\mathbf{T}=0)$	0	$-\frac{1}{8}-[1/2^{1/2}]\varepsilon_{O2,4y}(R_3;\mathbf{q}_1)+\varepsilon_{O2,4y}(R_7;\mathbf{q}_3)$	$-\frac{1}{4}+[1/2^{1/2}]\varepsilon_{O2,4z}(R_3;\mathbf{q}_1)+\varepsilon_{O2,4z}(R_7;\mathbf{q}_3)$
$O3(\mathbf{T}=0)$	$-\frac{1}{8}+\frac{1}{2}\varepsilon_{Ox}(R_8;\mathbf{q}_2)+\frac{1}{2}\varepsilon_{O1,3x}(R_7;\mathbf{q}_3)$	$\frac{1}{8}+\varepsilon_{Oy}(R_8;\mathbf{q}_2)-\varepsilon_{O1,3y}(R_7;\mathbf{q}_3)$	0
$O4(\mathbf{T}=0)$	0	$-\frac{1}{8}+[1/2^{1/2}]\varepsilon_{O2,4y}(R_3;\mathbf{q}_1)+\varepsilon_{O2,4y}(R_7;\mathbf{q}_3)$	$\frac{1}{4}+[1/2^{1/2}]\varepsilon_{O2,4z}(R_3;\mathbf{q}_1)-\varepsilon_{O2,4z}(R_7;\mathbf{q}_3)$

1.949 and 1.624 Å, respectively). A uniform expansion and contraction of alternate tetrahedra suggests that $\varepsilon_{O1,3x}(R_7;\mathbf{q}_3) = 2\varepsilon_{O1,3y}(R_7;\mathbf{q}_3) = 2\varepsilon_{O2,4y}(R_7;\mathbf{q}_3) = \varepsilon_{O2,4z}(R_7;\mathbf{q}_3) \simeq 0.025$.

The second $\mathbf{q} = 0$ mode is associated with an R_1 displacive modulation only, the atomic displacements of the framework atoms being given by

$$\mathbf{u}_{M1}(\mathbf{T}) = \mathbf{b}_p\varepsilon_{My}(R_1;\mathbf{q}_3)$$
$$\mathbf{u}_{M2}(\mathbf{T}) = -\mathbf{b}_p\varepsilon_{My}(R_1;\mathbf{q}_3)$$
$$\mathbf{u}_{Na1}(\mathbf{T}) = \mathbf{b}_p\varepsilon_{Nay}(R_1;\mathbf{q}_3)$$
$$\mathbf{u}_{Na2}(\mathbf{T}) = -\mathbf{b}_p\varepsilon_{Nay}(R_1;\mathbf{q}_3)$$
$$\mathbf{u}_{O1}(\mathbf{T}) = \mathbf{u}_{O2}(\mathbf{T}) = \mathbf{u}_{O3}(\mathbf{T}) = \mathbf{u}_{O4}(\mathbf{T}) = 0.$$

This mode is therefore incompatible with tetrahedral edge rotation and the amplitude $\varepsilon_{My}(R_1;\mathbf{q}_3)$ can be set at zero.

4.3. *Starting models*

Starting models for the Rietveld refinement of the orthorhombic phase can now be derived by summing the displacements of each atom due to the displacive modulations associated with each of the wavevectors $\mathbf{q}_1$, $\mathbf{q}_2$ and $\mathbf{q}_3$. Determination of the 24 displacive and one compositional degree of freedom associated with the above modulation functions is equivalent to determination of the structure of Na_2MgSiO_4. In order to derive a plausible starting model for Rietveld refinement, however, only those degrees of freedom associated with tetrahedral edge rotation and Mg/Si ordering need be taken into account. Taking only these degrees of freedom into account and re-expressing the above modulation functions in terms of the resultant unit cell gives the fractional coordinates listed in Table 2.

Relationships between the parameters listed in Table 2 and estimates of their magnitudes have been given earlier. Choosing, for example, $\varepsilon_{Mz}(R_3;\mathbf{q}_1) = 0.1140$, $\varepsilon_{O2,4z}(R_3;\mathbf{q}_1) = 0.2280$, $\varepsilon_{O2,4y}(R_3;\mathbf{q}_1) = 0.1205$, $\varepsilon_{Mx}(R_8;\mathbf{q}_2) = 0.0662$, $\varepsilon_{Ox}(R_8;\mathbf{q}_2) = 0.1324$, $\varepsilon_{Oy}(R_8;\mathbf{q}_2) = 0.0719$, $\varepsilon_{O1,3x}(R_7;\mathbf{q}_3) = 2\varepsilon_{O1,3y}(R_7;\mathbf{q}_3) = \varepsilon_{O2,4z}(R_7;\mathbf{q}_3) = 2\varepsilon_{O2,4y}(R_7;\mathbf{q}_3) = 0.0280$ and $\frac{1}{2}(f_{Mg} + f_{Si})a_M(R_7;\mathbf{q}_3) = \frac{1}{2}(-f_{Mg} + f_{Si})$ gives Mg—O distances in MgO_4 tetrahedra of 1.948 ± 0.019 Å and Si—O distances in SiO_4 tetrahedra of 1.626 ± 0.018 Å. These magnitudes clearly produce a good approximation to rigid-body rotation of the MgO_4 and SiO_4 tetrahedra. Note, however, that while the magnitudes of the displacements ε listed in Table 2 are known, their sign is not.

4.4. *Alternative plausible starting models*

The sign of the R_3, $\mathbf{q}_1 = \frac{1}{4}(202)^*_p$ mode can be chosen to be positive [*i.e.* $\varepsilon_{Mz}(R_3;\mathbf{q}_1) = 0.1140$, $\varepsilon_{O2,4z}(R_3;\mathbf{q}_1) = 0.2280$, $\varepsilon_{O2,4y}(R_3;\mathbf{q}_1) = 0.1205$], because an origin shift of $\frac{1}{2}(\mathbf{a}_p + \mathbf{c}_p)$ (with respect to the original C9-related cell, see Fig. 3) is equivalent to switching the sign of this mode with respect to the other two modes and, therefore, does not generate a distinct starting model. Four alternative and equally plausible starting models can, however, be generated by considering the possible sign combinations (+ +, + −, − + and − −) of the remaining two modes. The sign of the R_8, $\mathbf{q}_2 = \mathbf{b}^*$ mode, for example, can be either positive or negative, corresponding to anticlockwise or clockwise rotation around **c**. Hence, the signs of $\varepsilon_{Mx}(R_8;\mathbf{q}_2)$, $\varepsilon_{O1,3x}(R_8;\mathbf{q}_2)$ and $\varepsilon_{O1,3y}(R_8;\mathbf{q}_2)$ listed in §4.2 above can be switched to generate two distinct models. In addition, for each model generated in this way, a Si or Mg atom can be chosen to be at the unit-cell origin. This corresponds to reversing the sign of both the compositional and displacive components of the R_7, $\mathbf{q} = 0$ mode, thus expanding or contracting the M_1O_4 tetrahedron, depending on whether it is occupied by a Mg or Si atom.

Thus, four distinct and equally plausible starting models can be generated, the fractional coordinates of which (in space-group setting $Pn2_1a$) can be generated from Table 2 and from the magnitudes listed in the last paragraph of §4.2 above. The corresponding fractional coordinates in the standard $Pna2_1$ space-group setting can be generated from these *via* the relation (x, y, z) $Pna2_1 = (\frac{1}{8} + x, \frac{1}{4} - z, \frac{5}{8} + y)$ $Pn2_1a$.

4.5. *Structure refinement*

Specifications relevant to data collection and refinement of this and the other two structures are summarized in Table 3. The fractional coordinates of the four alternative starting models (+ +, + −, − + and − −) for the Rietveld refinement of Na_2MgSiO_4 are listed in Table

Table 3. *Specifications for data collection and refinement of the three structures*

Data collection	
Instrument	Siemens D-5000
Geometry	Bragg–Brentano
Radiation	Monochromated Cu $K\bar{\alpha}$
λ (Å)	1.5418
Mode	Step scan, 0.05° 2θ steps
2θ range (°)	10–80
Temperature (K)	293
Structure refinement	
Software	GSAS (Larson & Von Dreele, 1991)
Profile function	Type 2 Pseudo-Voigt
Profile variables	GW, LY, asym
Background	Cosine Fourier Series with six coefficients
Excluded regions	None

4 in the standard $Pna2_1$ space-group setting, together with the final refined coordinates for each model. As a result of the assumptions made in the derivation of these models, they are necessarily all equally plausible as far as the bond-valence sums for the framework Mg, Si and O atoms are concerned and, therefore, must be distinguished solely on the basis of refinement statistics.

The Rietveld refinement of this orthorhombic phase was carried out using the program *GSAS* (Larson & von Dreele, 1991) due to its ability to apply soft constraints to bond distances. Soft constraints of 1.624 ± 0.01 and 1.949 ± 0.05 Å were applied to the Si—O and Mg—O bond distances, respectively. The origin for the z coordinates was determined from the starting models and constrained accordingly. The thermal parameters of each parent structure-atom type were constrained to be equal.

The refined atomic parameters for the four models are given in Table 4. The ' − +' and '+ −' models, labelled models 2 and 3, respectively, gave R_{wp} and R_{Bragg} approximately 0.5% lower than the other two models, but could not be distinguished either on the basis of their refinement statistics (see Table 5) or bond-valence sums (see Table 4). Both Models 2 and 3 are equally chemically plausible. The observed, calculated and difference profiles for model 2 are presented in Fig. 8. The equivalent profiles for model 3 are indistinguishable from those of model 2 and are, therefore, not shown.

5. Refinement of the low carnegieite analogue $Na_{1.74}Mg_{0.79}Al_{0.15}Si_{1.06}O_4$

The underlying parent structure of this low carnegieite analogue phase is again a stuffed C9 derivative structure having $Fd3m$ symmetry and containing one $Na_{1.74}Mg_{0.79}Al_{0.15}Si_{1.06}O_4$ formula unit per primitive unit cell. The average occupancies of the framework metal and sodium-ion sites are therefore given by $f^{av}_{M1} = f^{av}_{M2} = 0.395f_{Mg} + 0.075f_{Al} + 0.530f_{Si}$ and $f^{av}_{Na1} = f^{av}_{Na2} = 0.870f_{Na}$.

Table 4. *Starting and final refined atomic coordinates for the four alternative starting models for the Rietveld refinement of orthorhombic Na_2MgSiO_4 ($Pna2_1$ setting)*

Orthorhombic, $Pna2_1$, $a = 10.835(5)$, $b = 5.279(12)$, $c = 7.068(8)$ Å, $D_x = 2.668\,g\,cm^{-3}$, $Z = 4$, Cu $K\alpha$, $\lambda = 1.5418$ Å, $\mu = 75.96\,cm^{-1}$, $F(000) = 319.87$.

	Models	x	y	z	U_{iso}	AV*
M1	*1,2*	*0.158*	*0.169*	*0.625*		
Si	1	0.154 (1)	0.210 (2)	0.622	0.042 (2)	3.82
Mg	2	0.158 (1)	0.204 (3)	0.621	0.041 (2)	2.02
M1	*3,4*	*0.092*	*0.169*	*0.625*		
Si	3	0.096 (1)	0.203 (2)	0.623	0.041 (2)	3.89
Mg	4	0.092 (1)	0.192 (3)	0.618	0.042 (2)	2.14
M2	*1,2*	*0.408*	*0.169*	*0.875*		
Mg	1	0.408 (1)	0.192 (3)	0.879 (3)	0.042 (2)	2.14
Si	2	0.404 (1)	0.202 (2)	0.876 (2)	0.041 (2)	3.90
M2	*3,4*	*0.342*	*0.169*	*0.875*		
Mg	3	0.342 (1)	0.204 (3)	0.878 (2)	0.041 (2)	2.01
Si	4	0.346 (1)	0.210 (2)	0.875 (2)	0.042 (2)	3.81
Na1	*1,2,3,4*	*0.125*	*0.250*	*0.125*		
Na1	1	0.163 (1)	0.219 (3)	0.152 (3)	0.058 (4)	0.94
	2	0.148 (2)	0.204 (4)	0.103 (3)	0.059 (3)	1.14
	3	0.086 (1)	0.240 (3)	0.153 (3)	0.060 (3)	0.97
	4	0.102 (2)	0.231 (4)	0.101 (3)	0.058 (4)	1.17
Na2	*1,2,3,4*	*0.375*	*0.250*	*0.375*		
Na2	1	0.398 (2)	0.231 (4)	0.396 (3)	0.058 (4)	1.16
	2	0.414 (1)	0.240 (3)	0.347 (3)	0.059 (3)	0.97
	3	0.352 (2)	0.204 (4)	0.397 (3)	0.060 (3)	1.14
	4	0.337 (1)	0.219 (3)	0.345 (3)	0.058 (4)	0.94
O1	*1*	*0.302*	*0.250*	*0.664*		
O1	1	0.301 (1)	0.272 (5)	0.661 (4)	0.053 (3)	2.03
	2	*0.330*	*0.250*	*0.692*		
	2	0.319 (2)	0.280 (4)	0.694 (2)	0.054 (3)	1.94
	3	*0.170*	*0.250*	*0.808*		
	3	0.181 (2)	0.281 (4)	0.805 (2)	0.054 (3)	1.91
	4	*0.198*	*0.250*	*0.836*		
	4	0.199 (1)	0.272 (5)	0.836 (4)	0.053 (3)	2.03
O2	*1*	*0.125*	*0.311*	*0.429*		
O2	1	0.100 (2)	0.337 (4)	0.428 (3)	0.053 (3)	2.22
	2	*0.125*	*0.367*	*0.401*		
	2	0.110 (2)	0.395 (2)	0.390 (4)	0.054 (3)	1.96
	3	*0.125*	*0.311*	*0.429*		
	3	0.152 (2)	0.330 (4)	0.431 (3)	0.054 (3)	2.07
	4	*0.125*	*0.367*	*0.401*		
	4	0.138 (2)	0.398 (2)	0.389 (3)	0.053 (3)	1.83
O3	*1*	*0.080*	*0.250*	*0.808*		
O3	1	0.068 (2)	0.258 (6)	0.807 (2)	0.053 (3)	1.96
	2	*0.052*	*0.250*	*0.836*		
	2	0.052 (1)	0.256 (5)	0.840 (4)	0.054 (3)	2.06
	3	*0.948*	*0.250*	*0.664*		
	3	0.948 (1)	0.244 (5)	0.660 (4)	0.054 (3)	2.05
	4	*0.920*	*0.250*	*0.692*		
	4	0.932 (2)	0.242 (6)	0.690 (2)	0.053 (3)	1.96
O4	*1*	*0.125*	*0.867*	*0.599*		
O4	1	0.138 (2)	0.898 (2)	0.609 (3)	0.053 (3)	1.85
	2	*0.125*	*0.811*	*0.572*		
	2	0.151 (2)	0.831 (4)	0.569 (3)	0.054 (3)	2.07
	3	*0.125*	*0.867*	*0.599*		
	3	0.110 (2)	0.895 (2)	0.609 (4)	0.054 (3)	1.98
	4	*0.125*	*0.811*	*0.572*		
	4	0.100 (2)	0.837 (4)	0.569 (3)	0.053 (3)	2.22

* Apparent valence or bond-valence sum (Brese & O'Keeffe, 1991).

Table 5. *Refinement statistics for the four alternative models of orthorhombic Na_2MgSiO_4*

Model	R_{wp}	R_p	R_{Bragg}
1	0.103	0.074	0.032
2	0.099	0.069	0.028
3	0.098	0.069	0.027
4	0.104	0.074	0.031

$R_{wp} = 100\Sigma w(y_{obs} - y_{calc})^2/\Sigma w y_{obs}^2$; $R_p = 100\Sigma|y_{obs} - y_{calc}|/\Sigma|y_{obs}|$; $R_{Bragg} = 100\Sigma|I_{obs} - I_{calc}|/\Sigma I$.

5.1. *Magnitude of the rotation about the* **a** *and* **c** *axes of the resultant structure*

Given the ideal cubic unit-cell parameter of 8.140 Å (as derived in §3.1 above), the observed cell parameters of $Na_{1.74}Mg_{0.79}Al_{0.15}Si_{1.06}O_4$ can be used to calculate the magnitude of the rotation angles θ_z and θ_x about the **a** and **c** axes of the resultant structure (see Figs. 1*a*, 3 and 7) as follows

$$a = 2a'\cos\theta_z = 8.140(2)^{1/2}\cos\theta_z$$
$$c = c'\cos\theta_x = (8.140/2^{1/2})\cos\theta_x$$
$$b = b'/(1 + \tan^2\theta_z + \tan^2\theta_x)^{1/2}$$
$$= 8.140/(1 + \tan^2\theta_z + \tan^2\theta_x)^{1/2}.$$

Since $a = 2c$ exactly, the magnitudes of the rotations about the **a** and **c** axes can be assumed to be identical (*i.e.* $\theta_x = \theta_z = \theta$). For a rotation angle $\theta = 22.55°$, the predicted resultant cell parameters are 10.637, 14.351 and 5.243 Å, all within ~ 2% of their experimentally determined values.

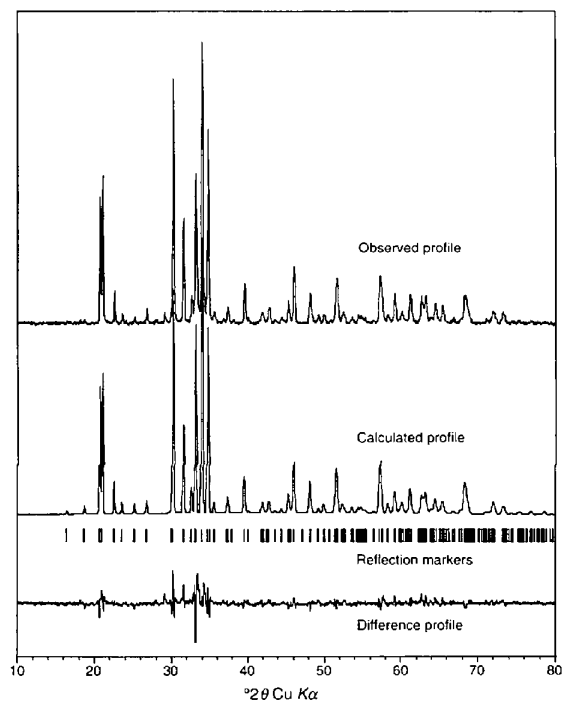

Fig. 8. Observed, calculated and difference profiles together with reflection markers for the final refined model of Na_2MgSiO_4.

5.2. *Irreducible representations and atomic displacement patterns associated with each of the various independent modulation wavevectors*

The phase of composition $Na_{1.74}Mg_{0.79}Al_{0.15}Si_{1.06}O_4$ is essentially isostructural with low carnegieite and, therefore, the resultant space-group symmetry allowed patterns of atomic displacement associated with each of the observed modulation wavevectors $\mathbf{q}_1 = \frac{1}{4}(020)^*_p$, $\mathbf{q}_2 = \frac{1}{4}(202)^*_p$, $\mathbf{q}_3 = \mathbf{q}_1 + \mathbf{q}_2 = \frac{1}{4}(222)^*_p$, $\mathbf{q}_4 = \mathbf{q}_1 - \mathbf{q}_2 = \frac{1}{4}(\bar{2}2\bar{2})^*_p$, $\mathbf{q}_5 = 2\mathbf{q}_1 = (010)^*_p$ and $\mathbf{q}_6 = \mathbf{0}$ are the same as those already given for low carnegieite in Withers & Thompson (1993) and hence will not be repeated here. Taking only those degrees of freedom associated with tetrahedral edge rotation and Mg/Si ordering into account and re-expressing in terms of the resultant $Pb2_1a$ unit cell gives the fractional coordinates listed in Table 6.

As in the case of low carnegieite, relationships between the parameters listed in Table 5 and estimates of their magnitudes can be obtained from a knowledge of the rotation angles (~22.6°) about the **a** and **c** axes and are given by

$$\varepsilon_{Mx}(\mathbf{q}_1) = \varepsilon_{Mz}(\mathbf{q}_2) = \varepsilon_{Mz}(\mathbf{q}_3,\mathbf{q}_4) = 0.0373,$$
$$\varepsilon_{O1,3y}(\mathbf{q}_1) = \varepsilon_{O2,4y}(\mathbf{q}_2) = \varepsilon_{O2,4z}(\mathbf{q}_2) = \varepsilon_{O2,4y}(\mathbf{q}_3,\mathbf{q}_4)$$
$$= \varepsilon_{O2,4z}(\mathbf{q}_3,\mathbf{q}_4) = 2\varepsilon_{Mx}(\mathbf{q}_1) = 0.0746.$$

$Pb2_1a$ resultant space-group symmetry allows compositional modulation of the metal- and Na-atom sites for $\mathbf{q}_5 = (010)^*_p$ and $\mathbf{q}_6 = 0$ modulation wavevectors. The extremely broad peak in the ^{29}Si spectrum of $Na_{1.74}Mg_{0.79}Al_{0.15}Si_{1.06}O_4$ (see Fig. 6*a*), however, indicates that the Si atoms have a range of chemical environments and consequently there cannot be long-range Mg/Si ordering. It is, therefore, a reasonable approximation to ignore these symmetry-allowed compositional degrees of freedom. Ignoring $\mathbf{q}_6 = 0$ compositional ordering and associated structural relaxation, however, is equivalent to raising the resultant space-group symmetry from $Pb2_1a$ to $Pbca$ (Withers & Thompson, 1993). The weak presence of $h0l$ reflections for which $l \neq 2n$ in Fig. 4(*a*) did not appear to be consistent with resultant $Pbca$ symmetry and, therefore, it was initially assumed that there must be some $\mathbf{q}_6 = 0$ compositional ordering.

The symmetry-allowed compositional modulation function associated with the $\mathbf{q}_6 = 0$ modulation wavevector is given by

$$f_{M1}(\mathbf{T}) = (0.395f_{Mg} + 0.075f_{Al} + 0.530f_{Si})\{1 + a_M(\mathbf{q}_6)\}$$
$$f_{M2}(\mathbf{T}) = (0.395f_{Mg} + 0.075f_{Al} + 0.530f_{Si})\{1 - a_M(\mathbf{q}_6)\}$$

Table 6. *Group theoretically derived fractional coordinates for* $Na_{1.74}Mg_{0.79}Al_{0.15}Si_{1.06}O_4$ *in* $Pb2_1a$, *as for low-carnegieite* $NaAlSiO_4$ *(Withers & Thompson, 1993)*

	Parent position	x	y	z
*M*1	$M1(\mathbf{T}=0)$	$0+\varepsilon_{Mx}(\mathbf{q}_1)$	0	$0+2\varepsilon_{Mz}(\mathbf{q}_3,\mathbf{q}_4)$
*M*2	$M1[\mathbf{T}=\frac{1}{2}(\mathbf{b}+\mathbf{c})]$	$\frac{1}{4}-\varepsilon_{Mx}(\mathbf{q}_1)$	$\frac{1}{4}$	$\frac{1}{2}-2\varepsilon_{Mz}(\mathbf{q}_2)$
*M*3	$M2(\mathbf{T}=0)$	$\frac{1}{4}+\varepsilon_{Mx}(\mathbf{q}_1)$	$\frac{1}{8}$	$0-2\varepsilon_{Mz}(\mathbf{q}_2)$
*M*4	$M2[\mathbf{T}=-\frac{1}{2}(\mathbf{a}+\mathbf{b})]$	$0+\varepsilon_{Mx}(\mathbf{q}_1)$	$-\frac{1}{8}$	$\frac{1}{2}+2\varepsilon_{Mz}(\mathbf{q}_3,\mathbf{q}_4)$
Na1	$Na1(\mathbf{T}=0)$	$\frac{1}{2}$	$\frac{1}{4}$	0
Na2	$Na1[\mathbf{T}=\frac{1}{2}(\mathbf{b}+\mathbf{c})]$	$\frac{3}{4}$	$\frac{1}{2}$	$\frac{1}{2}$
Na3	$Na2(\mathbf{T}=0)$	$\frac{3}{4}$	$\frac{3}{8}$	0
Na4	$Na2[\mathbf{T}=\frac{1}{2}(\mathbf{b}+\mathbf{c})]$	0	$\frac{5}{8}$	$\frac{1}{2}$
O1	$O1(\mathbf{T}=0)$	$\frac{1}{8}+2\varepsilon_{Mx}(\mathbf{q}_1)+\varepsilon_O(\mathbf{q}_6)$	$\frac{1}{16}-\varepsilon_{Mx}(\mathbf{q}_1)+\frac{1}{2}\varepsilon_O(\mathbf{q}_6)$	0
O2	$O1[\mathbf{T}=\frac{1}{2}(\mathbf{b}+\mathbf{c})]$	$\frac{3}{8}-2\varepsilon_{Mx}(\mathbf{q}_1)+\varepsilon_O(\mathbf{q}_6)$	$\frac{5}{16}+\varepsilon_{Mx}(\mathbf{q}_1)+\frac{1}{2}\varepsilon_O(\mathbf{q}_6)$	$\frac{1}{2}$
O3	$O2(\mathbf{T}=0)$	0	$-\frac{1}{16}-\varepsilon_{Mz}(\mathbf{q}_3,\mathbf{q}_4)-\frac{1}{2}\varepsilon_O(\mathbf{q}_6)$	$-\frac{1}{4}+4\varepsilon_{Mz}(\mathbf{q}_3,\mathbf{q}_4)-2\varepsilon_O(\mathbf{q}_6)$
O4	$O2[\mathbf{T}=\frac{1}{2}(\mathbf{b}+\mathbf{c})]$	$\frac{1}{4}$	$\frac{3}{16}+\varepsilon_{Mz}(\mathbf{q}_2)-\frac{1}{2}\varepsilon_O(\mathbf{q}_6)$	$\frac{1}{4}-4\varepsilon_{Mz}(\mathbf{q}_2)-2\varepsilon_O(\mathbf{q}_6)$
O5	$O3(\mathbf{T}=0)$	$-\frac{1}{8}+2\varepsilon_{Mx}(\mathbf{q}_1)-\varepsilon_O(\mathbf{q}_6)$	$\frac{1}{16}+\varepsilon_{Mx}(\mathbf{q}_1)+\frac{1}{2}\varepsilon_O(\mathbf{q}_6)$	0
O6	$O3[\mathbf{T}=\frac{1}{2}(\mathbf{b}+\mathbf{c})]$	$\frac{1}{8}-2\varepsilon_{Mx}(\mathbf{q}_1)-\varepsilon_O(\mathbf{q}_6)$	$\frac{5}{16}-\varepsilon_{Mx}(\mathbf{q}_1)+\frac{1}{2}\varepsilon_O(\mathbf{q}_6)$	$\frac{1}{2}$
O7	$O4(\mathbf{T}=0)$	0	$-\frac{1}{16}+\varepsilon_{Mz}(\mathbf{q}_3,\mathbf{q}_4)-\frac{1}{2}\varepsilon_O(\mathbf{q}_6)$	$\frac{1}{4}+4\varepsilon_{Mz}(\mathbf{q}_3,\mathbf{q}_4)+2\varepsilon_O(\mathbf{q}_6)$
O8	$O4[\mathbf{T}=\frac{1}{2}(\mathbf{b}+\mathbf{c})]$	$\frac{1}{4}$	$\frac{3}{16}-\varepsilon_{Mz}(\mathbf{q}_2)-\frac{1}{2}\varepsilon_O(\mathbf{q}_6)$	$\frac{3}{4}-4\varepsilon_{Mz}(\mathbf{q}_2)+2\varepsilon_O(\mathbf{q}_6)$

$$f_{\mathrm{Na1}}(\mathbf{T}) = 0.870 f_{\mathrm{Na}}\{1 + a_{\mathrm{Na}}(\mathbf{q}_6)\}$$
$$f_{\mathrm{Na2}}(\mathbf{T}) = 0.870 f_{\mathrm{Na}}\{1 - a_{\mathrm{Na}}(\mathbf{q}_6)\}.$$

For the purposes of obtaining a starting model for refinement, the magnitude of the framework metal-atom occupancy modulation $a_M(\mathbf{q}_6)$ was initially chosen so that $(0.395f_{\mathrm{Mg}} + 0.075f_{\mathrm{Al}} + 0.530f_{\mathrm{Si}})a_M(\mathbf{q}_6) = 0.395(f_{\mathrm{Mg}} - f_{\mathrm{Si}})$ such that $f_{M1}(\mathbf{T}) = 0.790f_{\mathrm{Mg}} + 0.075f_{\mathrm{Al}} + 0.135f_{\mathrm{Si}}$ and $f_{M2}(\mathbf{T}) = 0.925f_{\mathrm{Si}} + 0.075f_{\mathrm{Al}}$. The differently sized $Mg/Al/SiO_4$ and Si/AlO_4 tetrahedra can then be taken account of by ascribing a value of 0.010 to the parameter $\epsilon_O(\mathbf{q}_6)$ in Table 6.

5.3. *Alternative plausible starting models*

As for the orthorhombic phase, the magnitudes of the parameters $\varepsilon_{Mx}(\mathbf{q}_1)$,$\varepsilon_{Mz}(\mathbf{q}_2)$, $\varepsilon_{Mz}(\mathbf{q}_3,\mathbf{q}_4)$ and $\varepsilon_O(\mathbf{q}_6)$ are known, but their signs remain to be determined. Reversing the sign of $\varepsilon_O(\mathbf{q}_6)$ and switching the Mg-rich and Si-ion sites does not, in this case, generate a distinct starting model. The signs of $\varepsilon_{Mx}(\mathbf{q}_1)$ and $\varepsilon_{Mz}(\mathbf{q}_2)$ can also be freely chosen, since reversals in the signs of these parameters are equivalent to origin shifts of $\mathbf{b}_p$ and $\frac{1}{2}(\mathbf{a}+\mathbf{c})_p$, respectively. However, $\varepsilon_{Mz}(\mathbf{q}_3,\mathbf{q}_4)$ may be either positive or negative, thus generating two alternative starting models (see Withers & Thompson, 1993), labelled *A* and *B*. Both models have $\varepsilon_{Mx}(\mathbf{q}_1) = \varepsilon_{Mz}(\mathbf{q}_2) = -0.0373$ and $\varepsilon_O(\mathbf{q}_6) = 0.010$; for model *A*, $\varepsilon_{Mz}(\mathbf{q}_3,\mathbf{q}_4) = +0.0373$ and for model *B*, $\varepsilon_{Mz}(\mathbf{q}_3,\mathbf{q}_4) = -0.0373$. Substitution of these parameter values into Table 6 gives the fractional coordinates of two necessarily equally plausible starting models for the structure of $Na_{1.74}Mg_{0.79}Al_{0.15}Si_{1.06}O_4$.

5.4. *Structure refinement*

Initial refinements of both starting models were carried out in the space group $Pb2_1a$. When the sodium and framework metal-atom positions were released, however, the refinements diverged. Inspection of the calculated profiles showed a mismatch in the scale of the parent and satellite reflections, with the parent reflections undercalculating while the satellite reflections were on scale. The relative intensities of the calculated parent and satellite reflections depend on the amplitude of the rotation angles about the **a** and **c** axes of the resultant structure. The greater the magnitude of the rotation angles, the greater the amplitudes of the displacive modulations and, hence, the more intense the satellite reflections relative to the parent reflections of the undistorted structure.

In order to decrease the intensities of the satellite reflections relative to the parent reflections, it was therefore necessary to significantly reduce the magnitudes of the parameters $\varepsilon_{Mx}(\mathbf{q}_1)$, $\varepsilon_{Mz}(\mathbf{q}_2)$ and $\varepsilon_{Mz}(\mathbf{q}_3,\mathbf{q}_4)$ from 0.0373 in the original starting models to ~0.029. This corresponds to a decrease in the effective rotation angles about the **a** and **c** axes of the average structure from 22.6 to ~17.4°. At first this was a puzzling result to us as crystal chemistry dictates that the magnitude of the rotation angles must be of the order 22.6° in order to satisfy the local bonding requirements of the atoms in the structure. It was soon realized, however, that such a decrease in the effective rotation amplitude of the average structure could easily result from tetrahedral rotational disorder, *i.e.* stacking faults perpendicular to the resultant **a** and **c** axes, across which the signs of rotation of the tetrahedra are reversed relative to those in the rest of the structure. The ~25% decrease in apparent rotation angle is then simply a measure of the relative proportions of the faulted and unfaulted portions of the structure.

It is not clear whether this tetrahedral rotational disorder is responsible for the Mg/Si disorder apparent

from the broad solid-state ^{29}Si NMR signal (see Fig. 6*a*) or whether the latter disorder is a separate effect. In any event, it is clear that this phase exhibits significant disorder. It was therefore decided to assume random distribution of the Mg, Al and Si atoms, *i.e.* to raise the resultant space-group symmetry from $Pb2_1a$ to *Pbca*. The subsequent refinement was therefore carried out in this higher-symmetry space group, with $\varepsilon_O(\mathbf{q}_6)$ set at 0 and with $\varepsilon_{Mx}(\mathbf{q}_1)$, $\varepsilon_{Mz}(\mathbf{q}_2)$ and $\varepsilon_{Mz}(\mathbf{q}_3,\mathbf{q}_4)$ all initially put equal to –0.029. The standard setting of *Pbca* requires an origin shift of $\frac{3}{16}\mathbf{b} + \frac{1}{4}\mathbf{c}$ with respect to the origin used in Table 6. The resultant fractional atomic coordinates of this revised starting model with respect to the standard origin for space group *Pbca* are given in Table 7. The metal-atom sites *M*1 and *M*2 were given statistical occupancy and refined as (0.4325 Mg + 0.5675 Si) being electronically equivalent to 0.5 ($Mg_{0.79}Al_{0.15}Si_{1.06}$), and the two sodium site occupancies were set at 0.87 as required by stoichiometry. Soft contraints were placed on the *M*1—O and *M*2—O distances at 1.787 ± 0.05 Å, the average of 1.949 and 1.624 Å, the ideal distances in regular MgO_4 and SiO_4 tetrahedra, respectively. The thermal parameters of each parent structure-atom type were constrained to be equal. The refinement statistics at convergence were R_p = 0.061, R_{wp} = 0.083 and R_{Bragg} = 0.032.

As the refined model in this higher-symmetry space group gave an inordinately large U_{iso} of 0.089 (3) Å^2 for the interstitial sodiums, and as interstitial Na-atom positions would be expected to respond to local Si:Mg ordering, the two Na-atom sites were allowed to split equally, resulting in a significant improvement in the profile fit. The final refinement statistics for this split atom model were R_p = 0.056, R_{wp} = 0.077 and R_{Bragg} = 0.021. Excellent agreement between the observed and calculated profiles is shown in Fig. 9 with the only significant mismatch due to imperfect peak profile modelling for the parent 111 reflection. The final refined atomic parameters for this average structure are presented in Table 7.

6. Refinement of the *α*-cristobalite-related tetragonal phase

6.1. *Magnitude of the rotation about the* **a** *and* **c** *axes of the resultant structure*

Given the ideal cubic unit-cell parameter of 8.176 Å (as derived in §3.1 above), the observed cell parameters of $Na_{1.8}Mg_{0.9}Si_{1.1}O_4$ can be used to calculate the magnitude of the rotation angle θ (= θ_z = θ_x) about the **a** and **c** axes of the resultant structure (see Figs. 1*a*, 3 and 7) as follows

$$a = a'\cos\theta_z = 8.176/(2)^{1/2}\cos\theta_z = c = c'\cos\theta_x$$
$$= 8.176/(2)^{1/2}\cos\theta_x$$
$$b = b'/(1 + 2\tan^2\theta)^{1/2} = 8.176/(1 + 2\tan^2\theta)^{1/2}.$$

For a rotation angle θ = 22.40°, the predicted resultant cell parameters are $a = c$ = 5.345 and b = 7.064 Å, all within ~0.3% of their experimentally determined values.

6.2. *Irreducible representations and atomic displacement patterns associated with each of the various independent modulation wavevectors*

The only independent modulation wavevectors in the case of $Na_{1.8}Mg_{0.9}Si_{1.1}O_4$ are $\mathbf{q}_1 = (010)^*_I$ and $\mathbf{q}_2 = 0$.

6.2.1. *The* $\boldsymbol{q}_1 = \boldsymbol{b}^*$ *modulation.* The little co-group of this modulation wavevector is *mmm* itself. The corresponding irreducible representations are therefore as listed in Table 1. Only modes of R_4 and R_8 symmetry are compatible with a resultant space-group symmetry of $P4_12_12$ (note that in the setting of Fig. 3, the tetragonal axis is along **b**). Neither mode is compatible with compositional modulation of the framework metal atoms.

The most general pattern of atomic displacements associated with the R_8 irreducible representation, corresponding to tetrahedral edge rotation around **c**, is precisely the same as that already given in §4.2.2 above (except, of course, for the fact that $\mathbf{q}_2$ in that expression should be replaced by $\mathbf{q}_1$). The most general pattern of atomic displacements associated with the R_4 irreducible representation and corresponding to tetrahedral edge

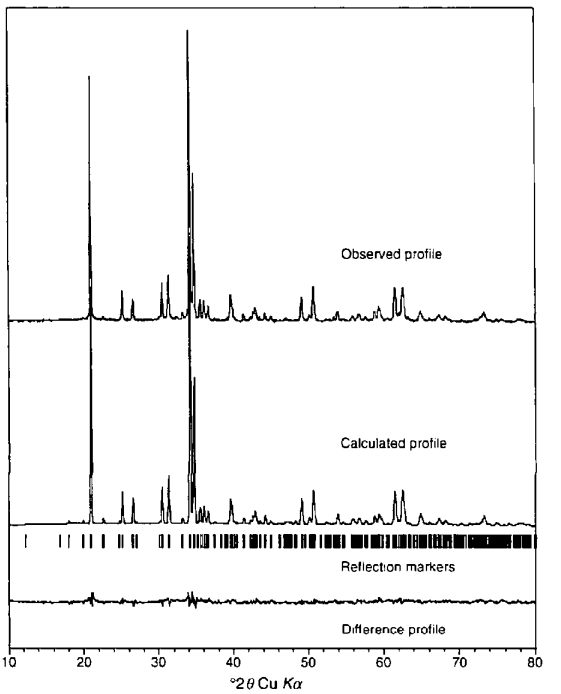

Fig. 9. Observed, calculated and difference profiles together with reflection markers for the final refined model of $Na_{1.74}Mg_{0.79}Al_{0.15}Si_{1.06}O_4$.

Table 7. *Starting and final refined atomic coordinates for the Rietveld refinement of orthorhombic* $Na_{1.74}Mg_{0.79}Al_{0.15}Si_{1.06}O_4$

Orthorhombic, *Pbca*, $a = 10.487(7)$, $b = 14.351(4)$, $c = 5.243(6)$ Å, $D_x = 2.643\,g\,cm^{-3}$, $Z = 8$, Cu $K\alpha$, $\lambda = 1.5418$ Å, $\mu = 76.70\,cm^{-1}$, $F(000) = 619.04$.

	x	y	z	U_{iso}	Previous label	Occupancy
M1	*0.971*	*0.813*	*0.692*		*M*1(T = 0)	0.4325Mg + 0.5675Si
*M*1	0.980 (1)	0.813 (1)	0.690 (2)	0.031 (2)		0.4325Mg + 0.5675Si
M2	*0.279*	*0.063*	*0.308*		*M*1[T = ½(b + c)]	0.4325Mg + 0.5675Si
*M*2	0.274 (1)	0.060 (2)	0.289 (1)	0.031 (2)		0.4325Mg + 0.5675Si
Na1	*0.500*	*0.063*	*0.750*		Na1(T = 0)	0.87
Na1	0.505 (4)	0.058 (2)	0.698 (7)	0.041 (4)		0.435
Na2	0.479 (3)	0.049 (2)	0.791 (7)	0.041 (4)		0.435
Na2	*0.750*	*0.313*	*0.250*		Na1[T = ½(b + c)]	0.87
Na3	0.744 (2)	0.306 (2)	0.170 (5)	0.041 (4)		0.435
Na4	0.788 (2)	0.326 (2)	0.311 (5)	0.041 (4)		0.435
O1	*0.067*	*0.904*	*0.750*		O1(T = 0)	1.0
O1	0.070 (1)	0.907 (1)	0.738 (3)	0.054 (3)		1.0
O2	*0.000*	*0.779*	*0.384*		O2(T = 0)	1.0
O2	0.026 (1)	0.786 (1)	0.367 (3)	0.054 (3)		1.0
O3	*0.250*	*0.971*	*0.116*		O2[T = ½(b + c)]	1.0
O3	0.237 (1)	0.956 (1)	0.129 (3)	0.054 (3)		1.0
O4	*0.817*	*0.846*	*0.750*		O2(T = 0)	
O4	0.818 (1)	0.840 (1)	0.809 (2)	0.054 (3)		1.0

rotation around **a** is given by

$$u_{M1}(\mathbf{T}) = \tfrac{1}{2}(-\mathbf{a}+\mathbf{c})_p\{\varepsilon_{Mz}(R_4;\mathbf{q}_1)\cos(2\pi\mathbf{q}_1.\mathbf{T})\}$$
$$u_{M2}(\mathbf{T}) = -\tfrac{1}{2}(-\mathbf{a}+\mathbf{c})_p\{\varepsilon_{Mz}(R_4;\mathbf{q}_1)\cos(2\pi\mathbf{q}_1.\mathbf{T})\}$$
$$u_{Na1}(\mathbf{T}) = \tfrac{1}{2}(-\mathbf{a}+\mathbf{c})_p\{\varepsilon_{Naz}(R_4;\mathbf{q}_1)\cos(2\pi\mathbf{q}_1.\mathbf{T})\}$$
$$u_{Na2}(\mathbf{T}) = -\tfrac{1}{2}(-\mathbf{a}+\mathbf{c})_p\{\varepsilon_{Naz}(R_4;\mathbf{q}_1)\cos(2\pi\mathbf{q}_1.\mathbf{T})\}$$
$$u_{O1}(\mathbf{T}) = u_{O3}(\mathbf{T}) = 0$$
$$u_{O2}(\mathbf{T}) = \tfrac{1}{2}(-\mathbf{a}+\mathbf{c})_p\{\varepsilon_{Oz}(R_4;\mathbf{q}_1)\cos(2\pi\mathbf{q}_1.\mathbf{T})\} - \mathbf{b}_p\{\varepsilon_{Oy}(R_4;\mathbf{q}_1)\cos(2\pi\mathbf{q}_2.\mathbf{T})\}$$
$$u_{O4}(\mathbf{T}) = \tfrac{1}{2}(-\mathbf{a}+\mathbf{c})_p\{\varepsilon_{Oz}(R_8;\mathbf{q}_1)\cos(2\pi\mathbf{q}_1.\mathbf{T})\} + \mathbf{b}_p\{\varepsilon_{Oy}(R_4;\mathbf{q}_1)\cos(2\pi\mathbf{q}_2.\mathbf{T})\}.$$

Tetragonal symmetry requires that the magnitude of rotation around **a** must be the same as that around **c**. Given a rotation angle of 22.4° about both axes, the magnitudes of the unknown parameters can be estimated to be $\epsilon_{Ox}(R_8;\mathbf{q}_1) = 2\varepsilon_{Mx}(R_8;\mathbf{q}_1) = 2\varepsilon_{Mz}(R_4;\mathbf{q}_1) = \varepsilon_{Oz}(R_4;\mathbf{q}_1) = 2\varepsilon_M = 0.1462$, $\varepsilon_{Oy}(R_8;\mathbf{q}_1) = \varepsilon_{Oy}(R_4;\mathbf{q}_1) = \varepsilon_{Oy} = 0.0777$.

6.2.2. *The $\mathbf{q}_2 = \mathbf{0}$ modulation.* The possibility of a $\mathbf{q}_2 = \mathbf{0}$ modulation wave must always be allowed for. The little co-group of this modulation wavevector is again *mmm*, the irreducible representations of which are also as listed in Table 1. None of these irreducible representations, however, are compatible with a resultant space-group symmetry of $P4_12_12$.

Starting models for the Rietveld refinement of this phase can now be derived by summing the contributions of the R_4 and R_8, $\mathbf{q}_1 = \mathbf{b}^*$ modes. Taking only those degrees of freedom associated with tetrahedral edge rotation into account and re-expressing the above modulation functions in terms of the resultant unit cell (see Fig. 3) gives the ideal fractional coordinates listed in Table 8.

6.3. *Alternative plausible starting models*

Reversing the sign of both the R_4 and R_8 modes is simply equivalent to an origin shift. Reversing the sign of one of the modes relative to the other simply generates the alternative $P4_32_12$ enantiomer. Hence, we are free to choose the sign of both modes to be positive. The Na atom again remains in its ideal position. Substitution of the parameters $2\varepsilon_M = 0.1462$ and $\varepsilon_{Oy} = 0.0777$ gives the starting model as listed in Table 7. The fractional coordinates in the standard setting of $P4_12_12$, as used in the refinement, are related to this group-theory-derived model *via* the transformation (x,y,z) standard setting = $(z + \frac{1}{4}, x + \frac{1}{4}, y)$.

6.4. *Structure refinement*

The starting model for the refinement was as derived above. Initially soft constraints of $d_{M-O} = 1.77 \pm 0.10$ Å

Table 8. *Starting and final refined atomic coordinates for the Rietveld refinement of α-cristobalite-related* $Na_{1.8}Mg_{0.9}Si_{1.1}O_4$

Orthorhombic, *Pbca*, $a = 10.487(7)$, $b = 14.351(4)$, $c = 5.243(6)$ Å, $D_x = 2.643\,g\,cm^{-3}$, $Z = 8$, Cu $K\alpha$, $\lambda = 1.5418$ Å, $\mu = 76.70\,cm^{-1}$, $F(000) = 619.04$.

Starting model:
Tetragonal, $P4_12_12$, $a = c = 5.330$, $b = 7.086$ Å

	x	y	z	Previous label	Occupancy
M	$0 + \varepsilon_M = 0.0731$	0	$0 + \varepsilon_M = 0.0731$	$M1(\mathbf{T} = 0)$	0.45Mg + 0.55Si
Na	0	$\frac{1}{2}$	0	Na1[$\mathbf{T} = -\frac{1}{2}(\mathbf{b} + \mathbf{c})$]	0.90
O	$-\frac{1}{4} + 2\varepsilon_{Ox} = -0.1038$	$\frac{1}{8} + \varepsilon_{Oy} = 0.2027$	0	O3($\mathbf{T} = 0$)	1.0

Refined and starting models (standard $P4_12_12$ setting):
Tetragonal, $P4_12_12$, $a = 5.330(6)$, $c = 7.086(5)$ Å, $D_x = 2.609\,g\,cm^{-3}$, $Z = 2$, Cu $K\alpha$, $\lambda = 1.5418$ Å, $\mu = 75.44\,cm^{-1}$, $F(000) = 155.94$.

	x	y	z	U_{iso}	Occupancy
M	*0.323*	*0.323*	*0.000*		0.45Mg + 0.55Si
M	0.304 (1)	0.304 (1)	0.000	0.038 (4)	0.45Mg + 0.55Si
Na	*0.250*	*0.250*	*0.500*		0.9
Na	0.287 (1)	0.287 (1)	0.500	0.075 (5)	0.9
O	*0.250*	*0.146*	*0.203*		1.0
O	0.234 (2)	0.126 (1)	0.197 (1)	0.046 (5)	1.0

were applied to the framework atoms, but these were released towards the end of the refinement. The thermal parameters of each parent structure-atom type were constrained to be equal. The final statistics for the refined model were $R_p = 0.063$, $R_{wp} = 0.080$ and $R_{Bragg} = 0.018$. The observed, calculated and difference profiles for this model are illustrated in Fig. 10 and the final refined atomic parameters listed in Table 8. The final refined values for the parameters $\varepsilon_{Ox}(R_8;\mathbf{q}_1) = \varepsilon_{Oz}(R_4;\mathbf{q}_1) = 0.126$ as opposed to the crystal chemically required 0.146, $\varepsilon_{Mx}(R_8;\mathbf{q}_1) = \varepsilon_{Mz}(R_4;\mathbf{q}_1) = 0.054$ rather than 0.073 and $\varepsilon_{Oy}(R_8;\mathbf{q}_1) = \varepsilon_{Oy}(R_4;\mathbf{q}_1) = \varepsilon_{Oy} = 0.072$ rather than 0.078 is consistent with the presence of some disorder, although to a lesser extent than for $Na_{1.74}Mg_{0.79}Al_{0.15}Si_{1.06}O_4$. It should be remembered, however, that this refined structural model is necessarily that of the average structure rather than the 'local' crystal structure of this phase.

7. Discussion

The corner-connected tetrahedral framework of the three sodium magnesiosilicates discussed in this paper each distort from the underlying C9-type parent structure *via* their own particular pattern of coupled tetrahedral edge rotations about the mutually orthogonal $[101]_p$ and $[\bar{1}01]_p$ (see Figs. 11 and 12 – the same setting as shown in Fig. 3 has been used in order to see the close relationship between these three structures). The magnitude of these tetrahedral edge rotations (~23°) about **a**′ and **c**′ are virtually identical for each tetrahedron and result in a reduction of the *M*—O—*M* bond angles from 180° in these distorted derivative structures. Note that rotation about $<\bar{1}01>_p$ of a particular tetrahedron in a $<101>_p$ row (<101> tetrahedral rows in Figs. 11 and

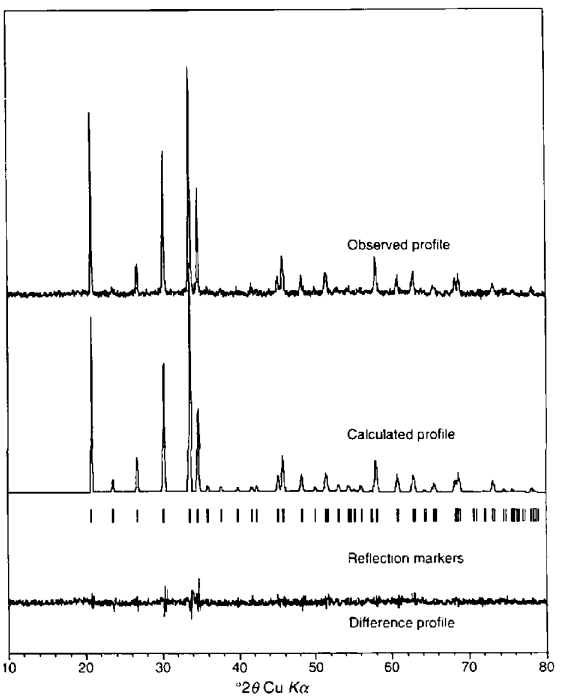

Fig. 10. Observed, calculated and difference profiles together with reflection markers for the final refined model of $Na_{1.8}Mg_{0.9}Si_{1.1}O_4$.

12 are delineated by the dashed lines) determines the direction of rotation of all other tetrahedra in that row, but places no constraints on the direction of rotation of the framework tetrahedra in neighbouring <101> tetrahedral rows. [It is this lack of correlation between the tetrahedral edge rotations of neighbouring <101> tetrahedral rows that gives rise to the strong sheets of diffuse intensity normal to <101> so characteristic of β-cristobalite (Withers *et al.*, 1989)].

The doubling of the **b** axis of the *Pbca* phase (see Fig. 3) relative to that of the other two phases is simply due to the different pattern of coupled tetrahedral edge rotations characteristic of that phase (as is clear from Figs. 11 and 12). The doubling of the **a** axes of the $Pn2_1a$ and *Pbca* phases relative to that of the $P4_12_12$ phase is again due to the different patterns of coupled tetrahedral edge rotations characteristic of these phases, but has not been represented in Fig. 11 to simplify structural comparison. Rotation about the $\mathbf{a}'$ axis in the case of the orthorhombic $Pn2_1a$ phase is associated with the $\frac{1}{4}(202)^*_p$ modulation wavevector, whereas rotation about the $\mathbf{a}'$ axis in the case of the pseudo-tetragonal *Pbca* phase is associated with the $\mathbf{q}_2 = \frac{1}{4}(202)^*_p$, $\mathbf{q}_3 = \frac{1}{4}(222)^*_p$ and $\mathbf{q}_4 = \frac{1}{4}(2\bar{2}2)^*_p$ modulation wavevectors. For each of these modulation wavevectors, $2\pi\mathbf{q}.\frac{1}{2}(\mathbf{a}+\mathbf{c})_p = \pi$, requiring that the sign of tetrahedral rotation reverses on translation by $\mathbf{a}' = \frac{1}{2}(\mathbf{a}+\mathbf{c})_p = \frac{1}{2}\mathbf{a}$ and giving rise to unit-cell doubling along $\mathbf{a}'$. As such tetrahedra obviously project on top of each other along $\mathbf{a}'$, for reasons of clarity only two adjacent tetrahedral layers perpendicular to the $\mathbf{a}'$ direction [those containing the M_1 ($\mathbf{T} = 0$) and M_2 ($\mathbf{T} = 0$) ions] are shown in Fig. 11. It is to

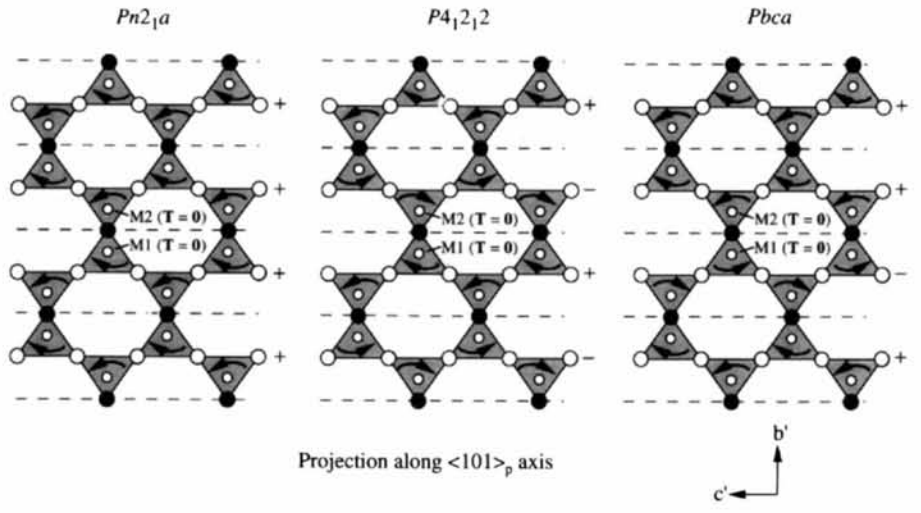

Fig. 11. Projection along the $[101]_p$ axis of the three structures showing their patterns of coupled tetrahedral edge rotation about $[101]_p$. The same setting as shown in Fig. 3 has been used in order to see the close relationship between the three structures. The + and – signs associated with each $[\bar{1}01]_p$ tetrahedral row indicate whether the associated framework cations move in the $+\mathbf{c}'$ or $-\mathbf{c}'$ direction. In the case of the $Pn2_1a$ and *Pbca* structures only two adjacent tetrahedral layers perpendicular to the $\mathbf{a}'$ direction [those containing the M_1 ($\mathbf{T} = 0$) and M_2 ($\mathbf{T} = 0$) ions] are shown. The directions of rotation of these framework tetrahedra are reversed every two tetrahedral layers, giving rise to the doubled **a** axes relative to that of the $P4_12_12$ phase.

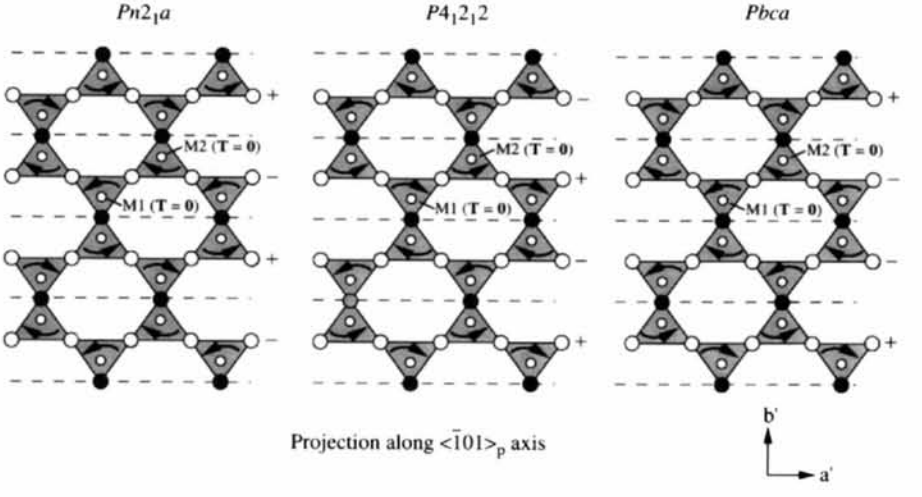

Fig. 12. Projection along the $[\bar{1}01]_p$ axis of the three structures showing their patterns of coupled tetrahedral edge rotation about $[\bar{1}01]_p$. The same setting as shown in Fig. 3 has been used in order to see the close relationship between the three structures. The + and – signs associated with each $[\bar{1}01]_p$ tetrahedral row indicate whether the associated framework cations move in the $+\mathbf{a}'$ or $-\mathbf{a}'$ direction.

be understood that the signs of rotation around $\mathbf{a}'$ of framework tetrahedra in the sheets perpendicular to the $\mathbf{a}'$ direction are reversed every two tetrahedral layers.

The only previously reported crystal structure for a cristobalite-related sodium magnesiosilicate is that of hydrothermally grown Na_2MgSiO_4 (Baur *et al.*, 1981). The $MgSiO_4$ corner-connected tetrahedral framework of this refined crystal structure can again be described in terms of a distortion of an underlying C9-type parent structure *via* coupled tetrahedral edge rotation about two mutually orthogonal $<110>_p$ axes (equivalent to the **b** and **c** axes in the setting used by Baur *et al.* (1981). Comparison of a [100] projection of the Baur *et al.* (1981) substructure with an [010] projection of β-$NaFeO_2$ (see Fig. 10*a* of O'Keeffe & Hyde, 1976) shows that the two crystal structures, in terms of their pattern of coupled tetrahedral edge rotations, are isomorphous, and therefore fundamentally different to the present structures. In the setting adopted by Baur *et al.* (1981) the corresponding space group would be $Pbn2_1$, with a = 7.015(2), b = 5.484(1) and c = 5.260(1) Å. Magnesium/silicon ordering in the case of the Baur *et al.* (1981) Na_2MgSiO_4 structure destroys the **b** glide perpendicular to **a** and reduces the space-group symmetry to monoclinic $P1n1$. The Baur *et al.* (1981) superstructure which results in a doubling of the **b** axis, while preserving overall symmetry as $P1n1$, is more elegantly described as a very small amplitude $\mathbf{q} = \frac{1}{2}\mathbf{b}^*$ modulation of the substructure, possibly driven by further compositional ordering, *e.g.* Na occupancy.

It should be clear from the preceding discussion that each of the new phases reported in this paper and the Na_2MgSiO_4 structure of Baur *et al.* (1981) are very closely related, differing only in the degree of framework metal and sodium ion ordering, and in the pattern of tetrahedral edge rotation about the orthogonal $[101]_p$ and $[\bar{1}01]_p$ axes. It might therefore be expected that all these structures should have very similar free energies and that conversion between them should not be too difficult. Given that the sense of rotation of any particular <101> tetrahedral row places no constraints on the direction of rotation of the framework tetrahedra in neighbouring <101> tetrahedral rows, it follows that it is theoretically possible to generate an almost infinite variety of β-cristobalite-related structures by changing the patterns of rotation of the framework tetrahedra about the orthogonal [101] and [$\bar{1}$01] axes of the C9 parent structure. The determined rotation patterns of the three recently synthesized sodium magnesiosilicate structures and the Baur *et al.* (1981) structure discussed in this paper represent only four of these possible types of distortion of the β-cristobalite structure.

References

Bärnighausen, H. (1980). *Commun. Math. Chem.* **9**, 139–175.

Baur, W. H., Ohta, T. & Shannon, R. D. (1981). *Acta Cryst.* B**37**, 1483–1491.

Bertaut, E. F. & Blum, P. (1954). *C. R. Acad. Sci.* **239**, 429–431.

Bertaut, E. F., Delapalme, A., Bassi, G., Durif-Varambon, A. & Joubert, J.-C. (1965). *Bull. Soc. Fr. Minér. Crist.* **88**, 103–108.

Bradley, C. J. & Cracknell, A. P. (1972). *The Mathematical Theory of Symmetry in Solids*. Oxford University Press.

Brese, N. E. & O'Keeffe, M. (1991). *Acta Cryst.* B**47**, 192–197.

Brown, I. D. & Altermatt, D. (1985). *Acta Cryst.* B**41**, 244–247.

Buerger, M. J. (1954). *Am. Mineral.* **39**, 600–614.

Dollase, W. A. (1965). *Z. Kristallogr.* **121**, 369–377.

Foris, C. M., Zumsteg, F. C. & Shannon, R. D. (1979). *J. Appl. Cryst.* **12**, 405–406.

Joubert-Bettan, C. A., Lachenal, R., Bertaut, E. F. & Parthé, E. (1969). *J. Solid State Chem.* **1**, 1–5.

Kosten, K. & Arnold, H. (1980). *Z. Kristallogr.* **152**, 119–133.

Larson, A. C. & von Dreele, R. B. (1991). *GSAS. The General Structure Analysis System*. Los Alamos National Laboratory, Los Alamos, New Mexico, USA.

Lippmaa, E., Mägi, M., Samoson, A., Tarmak, M. & Engelhardt, G. (1981). *J. Am. Chem. Soc.* **103**, 4992–4996.

O'Keeffe, M. & Hyde, B. G. (1976). *Acta Cryst.* B**32**, 2923–2936.

Pérez-Mato, J. M., Madariaga, G., Zúñiga, F. J. & Garcia Arribas, A. (1987). *Acta Cryst.* A**43**, 216–226.

Shannon, R. D. (1979). *Phys. Chem. Miner.* **4**, 139–148.

Shannon, R. D. & Berzins, I. (1979). *Mater. Res. Bull.* **14**, 361–367.

Thompson, J. G., Withers, R. L., Whittaker, A. K., Traill, R. M. & Fitz Gerald, J. D. (1993). *J. Solid State Chem.* **104**, 59–73.

Vielhaber, E. & Hoppe, R. (1969). *Z. Anorg. Allg. Chem.* **369**, 14–32.

Withers, R. L. & Thompson, J. G. (1993). *Acta Cryst.* B**49**, 614–626.

Withers, R. L., Thompson, J. G. & Welberry, T. R. (1989). *Phys. Chem. Miner.* **16**, 517–523.

Wyckoff, R. W. G. (1925). *Am. J. Sci.* **209**, 448–459.